

LA-UR-14-26657

Approved for public release; distribution is unlimited.

Title: Total Reaction Cross Section Models in CEM and MCNP6 in the Intermediate-Energy Range (>1 MeV), LANL Summer 2014 Internship Report

Author(s): Kerby, Leslie Marie
Mashnik, Stepan Georgievich

Intended for: Report

Issued: 2014-09-02 (rev.1)

Disclaimer:

Los Alamos National Laboratory, an affirmative action/equal opportunity employer, is operated by the Los Alamos National Security, LLC for the National Nuclear Security Administration of the U.S. Department of Energy under contract DE-AC52-06NA25396. By approving this article, the publisher recognizes that the U.S. Government retains nonexclusive, royalty-free license to publish or reproduce the published form of this contribution, or to allow others to do so, for U.S. Government purposes. Los Alamos National Laboratory requests that the publisher identify this article as work performed under the auspices of the U.S. Department of Energy. Los Alamos National Laboratory strongly supports academic freedom and a researcher's right to publish; as an institution, however, the Laboratory does not endorse the viewpoint of a publication or guarantee its technical correctness.

Total Reaction Cross Section Models in CEM and MCNP6 in the Intermediate-Energy Range (> 1 MeV)

Leslie M. Kerby

University of Idaho, Idaho Falls, Idaho USA and

Los Alamos National Laboratory, Los Alamos, New Mexico USA

Stepan G. Mashnik

Los Alamos National Laboratory, Los Alamos, New Mexico USA

(LANL Summer 2014 Internship Report, LA-UR-14-26657)

(Dated: August 28, 2014)

CONTENTS

I. Introduction	3
II. Brief Review of Select Total Reaction Cross Section Models and Their Use in Spallation and Transport Codes	3
III. Overview of the CEM Model	7
IV. Previous Investigations of Total Reaction Cross Section Models	9
V. Comparison of Total Reaction Cross Section Models	9
A. Neutron-Induced Reactions	9
B. Proton-Induced Reactions	16
C. Heavy-Ion Induced Reactions	17
VI. Implementation of NASA Cross Section Model into MEM	24
A. Emission Width, Γ_j , Calculation	24
B. Kalbach Systematics	30
C. Gauss-Laguerre Quadrature	38
VII. Results	38
VIII. Conclusion	39
IX. Acknowledgments	42
X. References	43

I. INTRODUCTION

Total reaction cross section models have a significant impact on the predictions and accuracy of spallation and transport codes. The Cascade Exciton Model (CEM) code CEM03.03 [1] and the Monte Carlo N-Particle transport code (MCNP6) [2], both developed at Los Alamos National Laboratory (LANL), each use such cross sections for different purposes. While total reaction cross sections are used throughout the transport and spallation models, there are two main utilizations. MCNP6 uses total reaction cross sections to determine where a reaction occurs (thru the mean-free path length), and then with what nucleus the projectile interacts with, and lastly what type of interaction it is (inelastic or elastic). CEM uses total reaction cross sections as *inverse* cross sections to predict what the excited nucleus emits.

The current inverse cross sections used in the preequilibrium and evaporation stages of CEM are based on the Dostrovsky model, published in 1959 [3]. Better cross section models are available now [4–13]. MCNP6 uses an update of the Barashenkov and Polanski (B&P) cross section model [13] as described briefly in [14, 15] to calculate the mean-free path length for neutrons, protons, and light fragments up to ${}^4\text{He}$. It uses a parameterization based on a geometric cross section for light fragments above ${}^4\text{He}$. Implementing better cross section models in CEM and MCNP6 should yield improved results of particle spectra and total production cross sections, among other results.

This cross section development work is part of a larger project aimed at enabling CEM to produce high-energy light fragments [16–18]. Figs. 1 and 2 illustrate two examples of results of that project. For some reactions we obtained good results (i.e., Fig. 1), and for other reactions, while our results showed improvement, they could still be better (i.e., Fig. 2). We determined to upgrade the inverse cross section models used to see if we could improve these results further.

II. BRIEF REVIEW OF SELECT TOTAL REACTION CROSS SECTION MODELS AND THEIR USE IN SPALLATION AND TRANSPORT CODES

The current inverse cross sections in CEM are based on the Dostrovsky model [3]. It is based on the strong absorption model and its general form is as shown in Eq. 1.

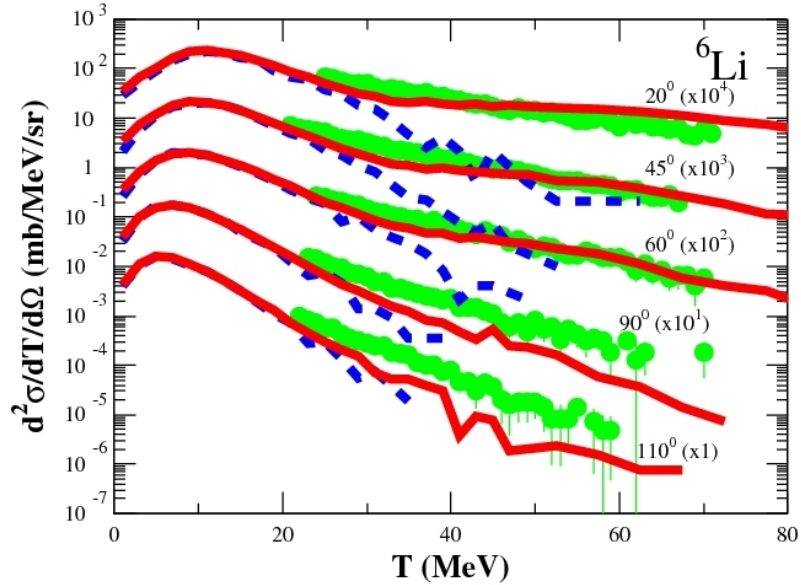


FIG. 1. Comparison of experimental data by Machner *et al.* [19] (green points) with results from the unmodified CEM03.03 (blue dotted lines) and the modified–MEM CEM03.03 [17, 18] (red solid lines) for 200 MeV $p + {}^{27}\text{Al} \rightarrow {}^6\text{Li} + \dots$

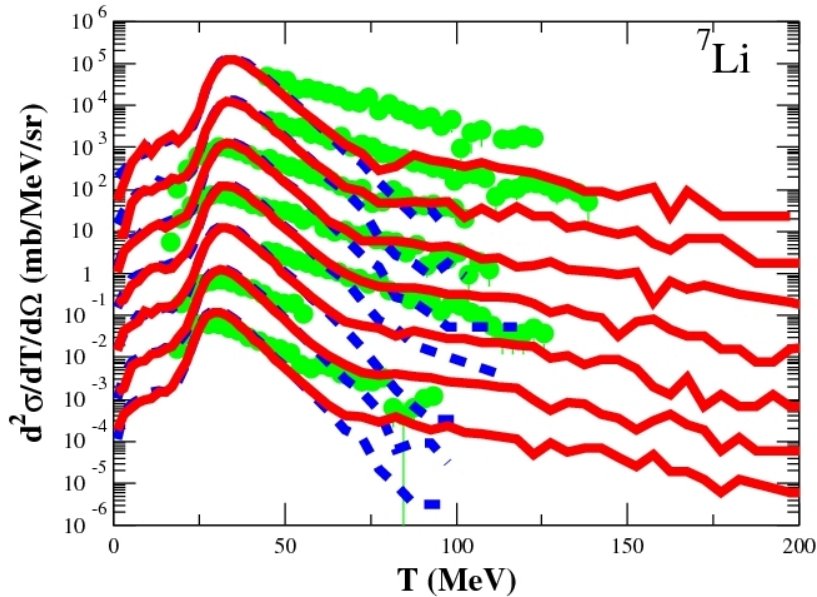


FIG. 2. Comparison of experimental data by Budzanowski *et al.* [20] (green points) with results from the unmodified CEM03.03 (blue dashed lines) and the modified-MEM CEM03.03 [17, 18] (red solid lines) for 1200 MeV $p + {}^{197}\text{Au} \rightarrow {}^7\text{Li} + \dots$

$$\sigma_{Dost.} = \pi r_0^2 A^{2/3} \alpha_j \left(1 - \frac{V_j}{E}\right). \quad (1)$$

The Dostrovsky model was not intended for use above about 50 MeV/nucleon, and is not very suitable for emission of fragments heavier than ${}^4\text{He}$. Better total reaction cross section models are available today, most notably the NASA model [4–6]. The NASA (or Tripathi et al.) model is also based on the strong absorption model and its general form is shown in Eq. 2. The NASA cross section attempts to simulate several quantum-mechanical effects, such as the optical potential for neutrons and collective effects like Pauli blocking. (For more details, see Refs. [4–6].)

$$\sigma_{NASA} = \pi r_0^2 (A_P^{1/3} + A_T^{1/3} + \delta_E)^2 \left(1 - R_c \frac{B}{E_{cm}}\right) X_m. \quad (2)$$

There are other recently proposed total reaction cross section models, most notably those by Shen, et al. [7], and Takechi, et al. [8], amongst others [9–13].

The FLUKA and PHITS transport codes teams have recently been analyzing their total reaction cross sections as well. Fig. 3 is adopted from a paper exploring a new total reaction cross section used in PHITS: the hybrid Kurotama model [21]. This model is a combination of the Black Sphere model [9] and the NASA model [4–6]. It is compared to “Tripathi,” who is the lead author of the NASA cross section model. Fig. 4 is adopted from a paper comparing a number of different cross section models, most notably those in FLUKA, and Tripathi (or NASA) again, and several other recently developed models [22]. In these studies the NASA model matches the experimental data, in general, better than the other cross section models studied.

PHITS uses the NASA model as its default cross section model, but Shen can be specified as an option [22]. FLUKA uses a modified version of the NASA model as its cross section model [23]. GEANT4 has the option to use NASA, or a number of other cross section models such as Shen [7] or Sihver [24], or the Axen-Wellisch [25] cross section parameterizations for high-energy hadronic interactions. See Ref. [26, 27] for more details on the total reaction cross section models used in PHITS, FLUKA and GEANT4.

In the recent Ref. [28], Krylov et al., compares proton spectra as calculated by GEANT4, SHIELD, and MCNPX 2.6 for relativistic heavy-ion collisions. Fig. 5 is an example of their findings. A newer (and better) version of MCNPX is now available, but these results

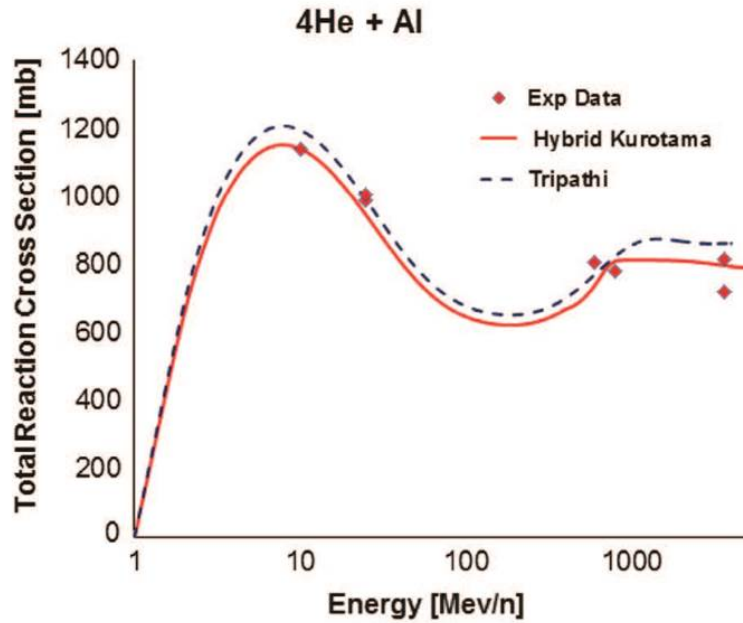


FIG. 3. Total reaction cross section by energy, comparing the Hybrid Kurotama and NASA (Tripathi) models as shown in [21].

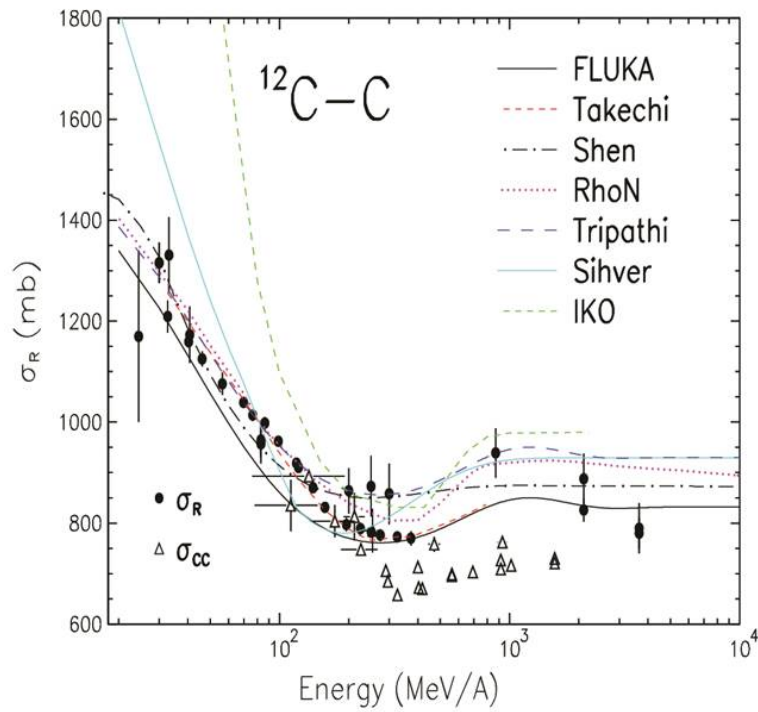


FIG. 4. Total reaction cross section by energy, comparing several different models, as shown in [22].

demonstrate the need for updated cross section models within CEM and MCNP6.

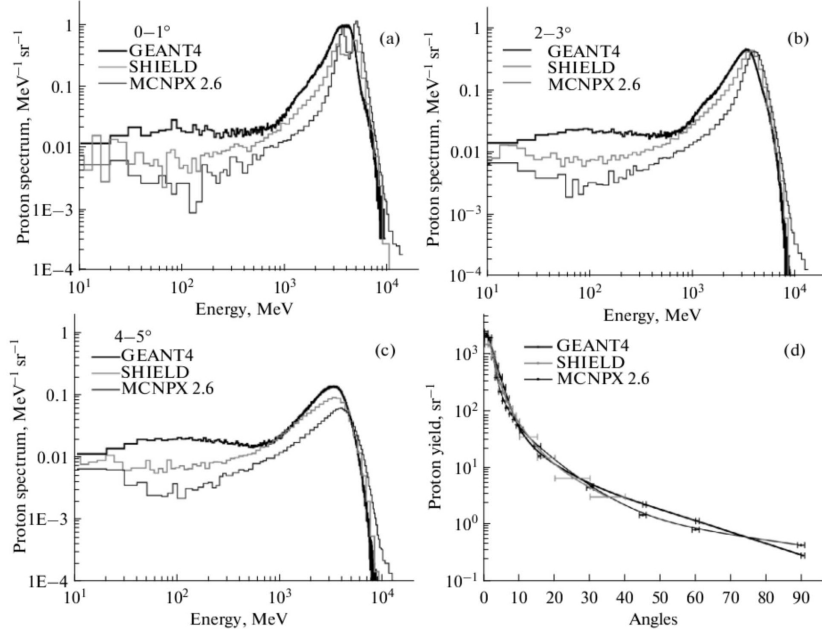


FIG. 5. (a)–(c) a comparison of the secondary proton spectra for the reactions ^{197}Au (4.5 GeV/n) + ^{nat}Fe simulated by the GEANT4, SHIELD, and MCNPX 2.6 codes. (d) a comparison of the angular distributions of protons for the reactions ^{197}Au (4.5 GeV/n) + ^{nat}Fe ; adopted from Ref. [28].

III. OVERVIEW OF THE CEM MODEL

As a rule, a reaction begins with the IntraNuclear Cascade, referred to as either the INC or as the Cascade (see Fig. 6). The incident particle or nucleus (in the case of using LAQGSM) enters the target nucleus and begins interacting with nucleons, scattering off them and also often creating new particles in the process. The incident particle and all newly created particles are followed until they either escape from the nucleus or reach a threshold energy (roughly 10-30 MeV per nucleon) and are then considered “absorbed” by the nucleus.

The preequilibrium stage uses an extension of the Modified Exciton Model (MEM) [29, 30] to determine emission of protons, neutrons, and fragments up to ^4He from the residual nucleus. This stage can have a highly excited residual nucleus undergoing dozens of exciton transitions and particle emissions. The preequilibrium stage ends when the residual nucleus

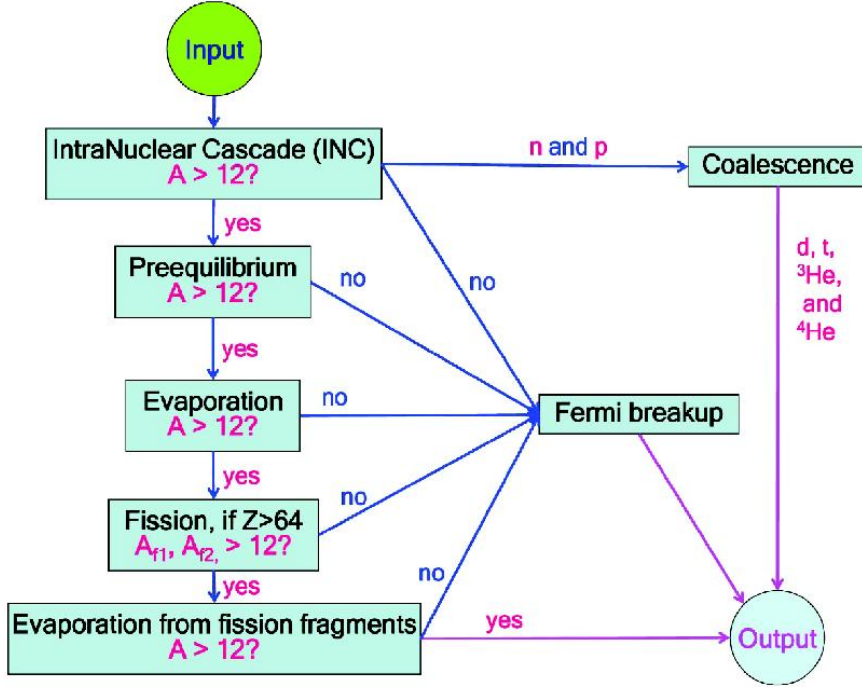


FIG. 6. Flowchart of nuclear-reaction calculations by CEM03.03 [16].

is practically as likely to have a $\Delta n = +2$ exciton transaction as a $\Delta n = -2$ exciton transaction.

In the evaporation stage, neutrons and protons in the outer shells of the residual nucleus can “evaporate” off, either singly or as fragments. The CEM evaporation stage is modeled after Furihata’s Generalized Evaporation Model (GEM2) [31], and can emit light fragments up to ^{28}Mg .

During and after evaporation, the code looks to see if we have an isotope that has $Z \geq 65$ and is fissionable. If it is, and there is fission, then the code follows the evaporation stage for the fission fragments.

There are two models that are not directly part of this linear progression: Coalescence and Fermi break-up (see Fig. 6). The Cascade stage only emits neutrons, protons, and pions (and other particles, in the case of using LAQGSM at high energies), so the coalescence model “coalesces” some of the neutrons and protons produced during the INC into larger fragments, by comparing their momenta. If their momenta are similar enough then they coalesce. The current coalescence model can only coalesce up to a ^4He fragment, the same as the standard preequilibrium stage [1]. The Fermi break-up is an oversimplified multifragmentation model that is fast and accurate for small atomic numbers, so we use it when the residual mass

number is less than or equal to 12.

IV. PREVIOUS INVESTIGATIONS OF TOTAL REACTION CROSS SECTION MODELS

Stepan Mashnik with collaborators [32, 33] and Dick Prael with coauthors [15, 34] previously conducted an extensive comparison of the NASA [4–6], Tsang *et al.* [11], Dostrovsky *et al.* [3], Barashenkov and Polansky (CROSEC) [13], and Kalbach [12] systematics for inverse cross sections. Fig. 7 illustrates some results from the study [32]. They also studied the B&P model (CROSEC) [13]. Figs. 8 to 12 illustrate more results, for 17 targets-nuclei from ^7Be to ^{238}U from the studies [32, 33]. Their results found that the NASA cross section model was superior, in general, to the other available cross section models.

V. COMPARISON OF TOTAL REACTION CROSS SECTION MODELS

Here, we built in CEM03.03F the NASA (Tripathi) model [4–6] and the models used in the preequilibrium (labeled Dostrovsky) and the evaporation stages (or GEM2) of CEM03.03, and also compared some reactions to calculations from the Barashenkov and Polanski (B&P) systematics [13], and, for comparison, to two neutron- and proton-induced reactions cross sections calculations by MCNP6 [2]. Note that MCNP6 uses currently an updated and improved version of the initial Barashenkov and Polanski (B&P) systematics [13], as outlined briefly in Refs. [13, 14], to simulate the mean-free path length of nucleons in the matter.

A. Neutron-Induced Reactions

Fig. 13 displays the total reaction cross section for $n + ^{208}\text{Pb}$, as calculated by the NASA, Dostrovsky, GEM2, and B&P models, and compared to calculations by MCNP6 and experimental data. There are several things to notice: 1) the Dostrovsky and GEM2 (also a Dostrovsky-based model) both approach asymptotic values very quickly—thus they are not as useful at their constant values, and 2) the NASA model, while much better at predicting the reaction cross section throughout the energy spectrum, falls to zero at low energies. This is unphysical to use for an inverse cross section, because neutrons are emitted

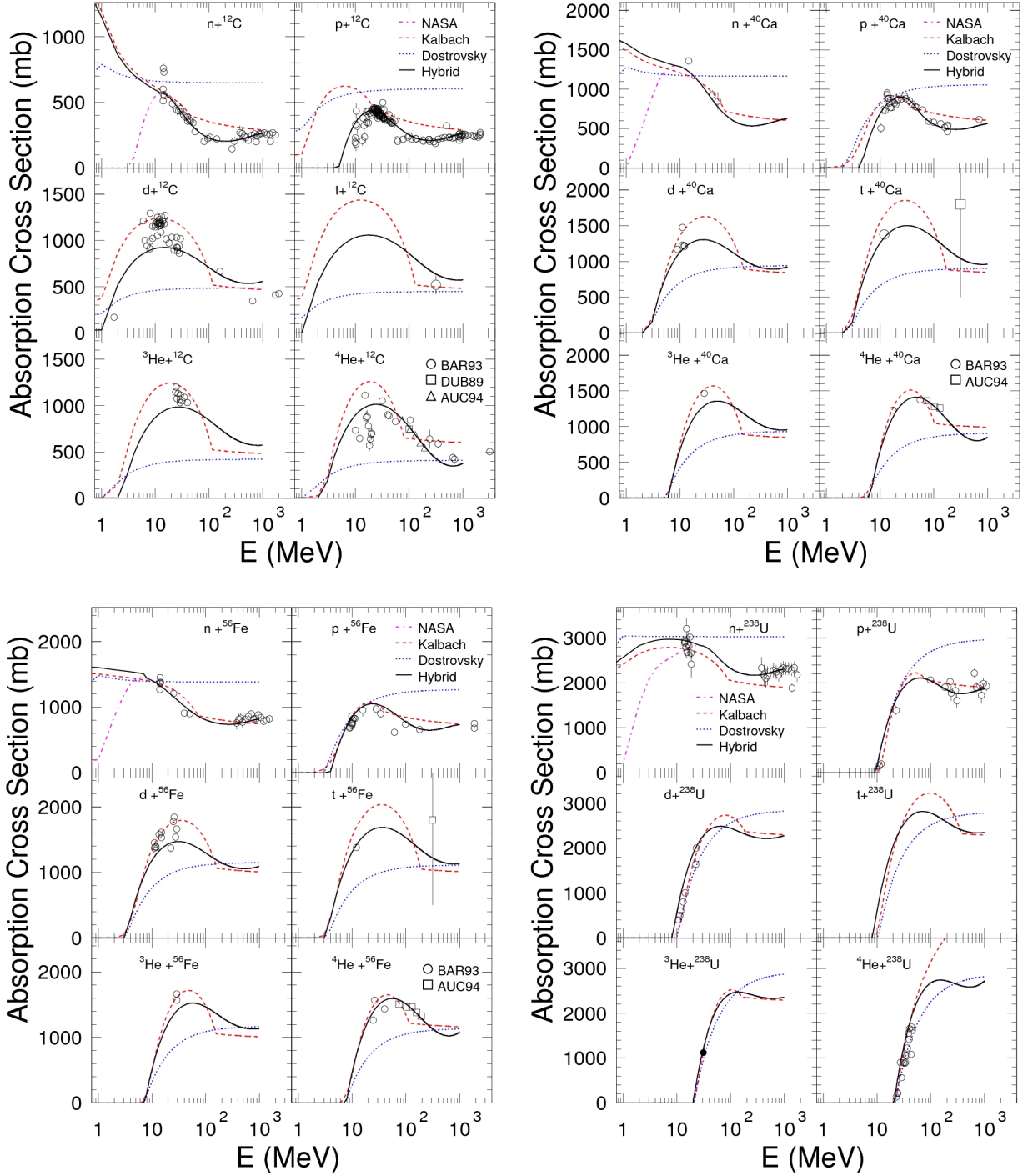


FIG. 7. Absorption cross section by energy for various reactions, as calculated in Ref. [32] by the NASA [4–6], Kalbach [12], and Dostrovsky [3] systematics, as well as with a “Hybrid approach” suggested in [32] to account for both NASA [5] and Kalbach [12] systematics, in case on neutron-induced reactions.

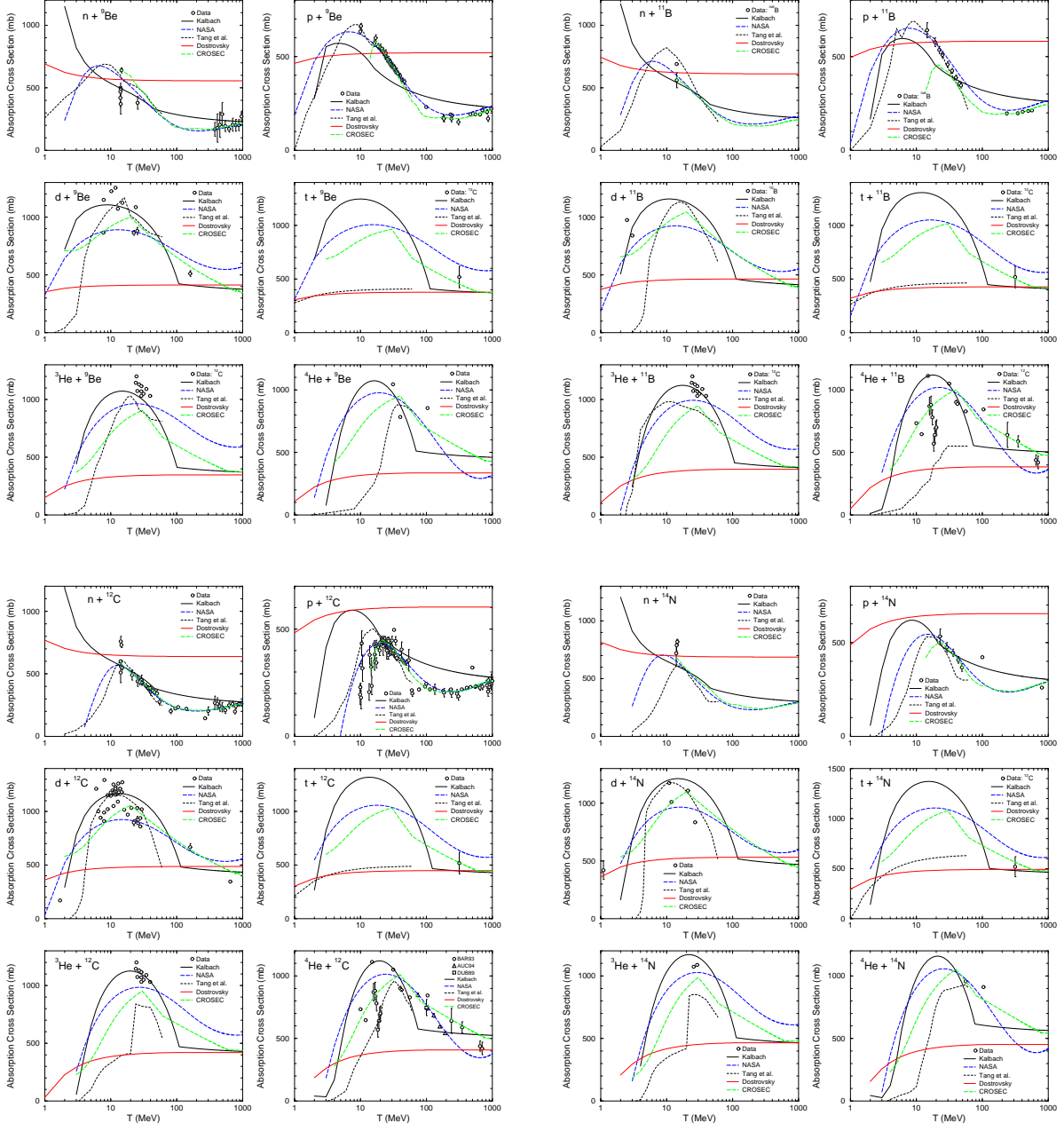


FIG. 8. Examples of total reaction cross section on target-nuclei ${}^9\text{Be}$, ${}^{11}\text{B}$, ${}^{12}\text{C}$, and ${}^{14}\text{N}$ studied in Refs. [32, 33] with Kalbach [12], NASA [4–6], Tsang *et al.* [11], Dostrovsky *et al.* [3], and Barashenkov and Polansky (CROSEC) [13] systematics compared with experimental data (references on experimental data can be found in [32]).

with low energies, and therefore this is something we need to alter in the NASA model to be able to apply it to inverse cross sections.

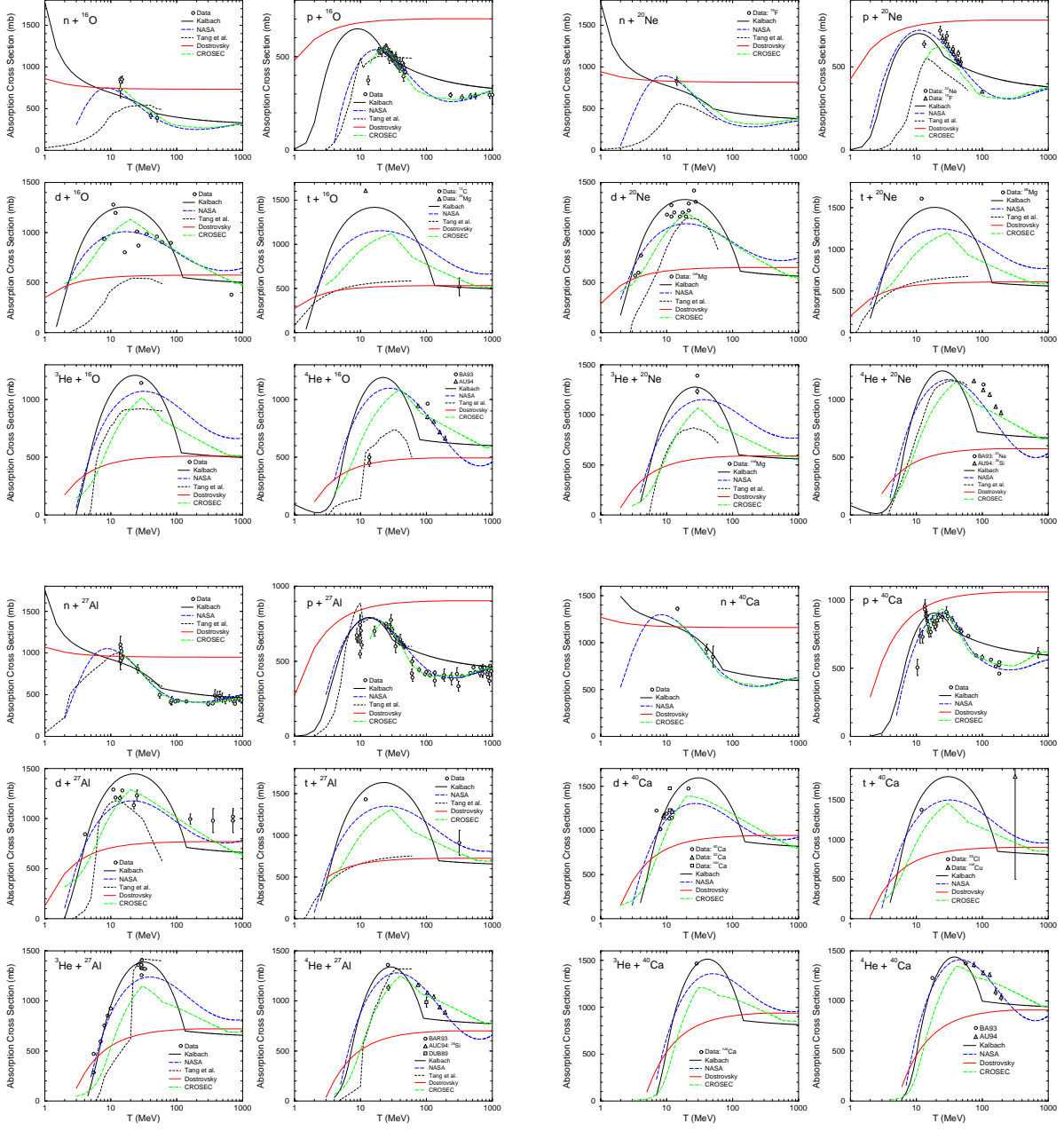


FIG. 9. Examples of total reaction cross section on target-nuclei ^{16}O , ^{20}Ne , ^{27}Al , and ^{40}Ca studied in Refs. [32, 33] with Kalbach [12], NASA [4–6], Tsang *et al.* [11], Dostrovsky *et al.* [3], and Barashenkov and Polansky (CROSEC) [13] systematics compared with experimental data (references on experimental data can be found in [32]).

Fig. 14 displays the total reaction cross section for $\text{n} + ^{119}\text{Sn}$, ^{63}Cu , ^{27}Al , and ^{12}C , as calculated by the NASA, Dostrovsky, and GEM2 models, and compared to experimental

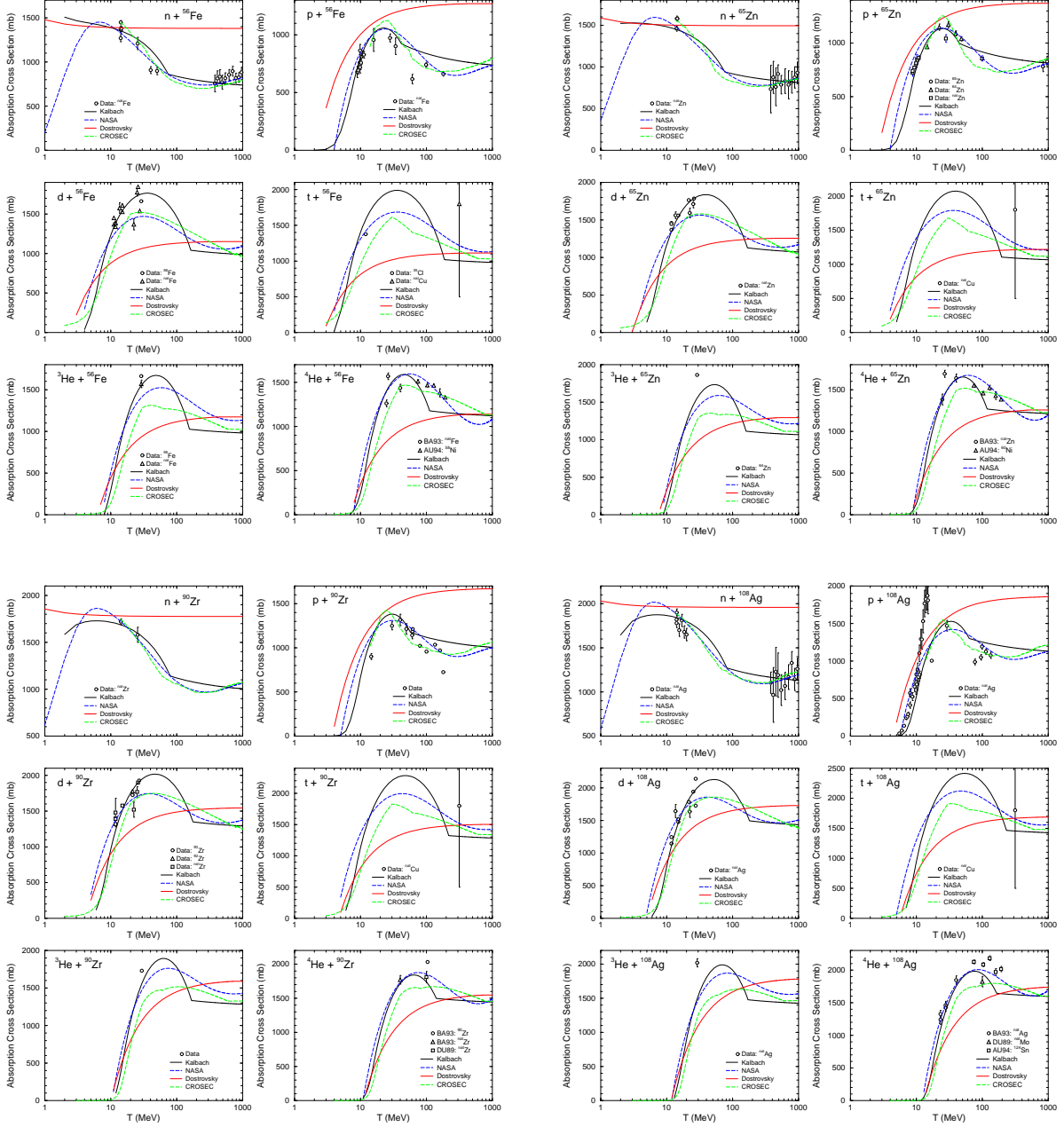


FIG. 10. Examples of total reaction cross section on target-nuclei ^{56}Fe , ^{65}Zn , ^{90}Zr , and ^{108}Ag studied in Refs. [32, 33] with Kalbach [12], NASA [4–6], Tsang *et al.* [11], Dostrovsky *et al.* [3], and Barashenkov and Polansky (CROSEC) [13] systematics compared with experimental data (references on experimental data can be found in [32]).

data.

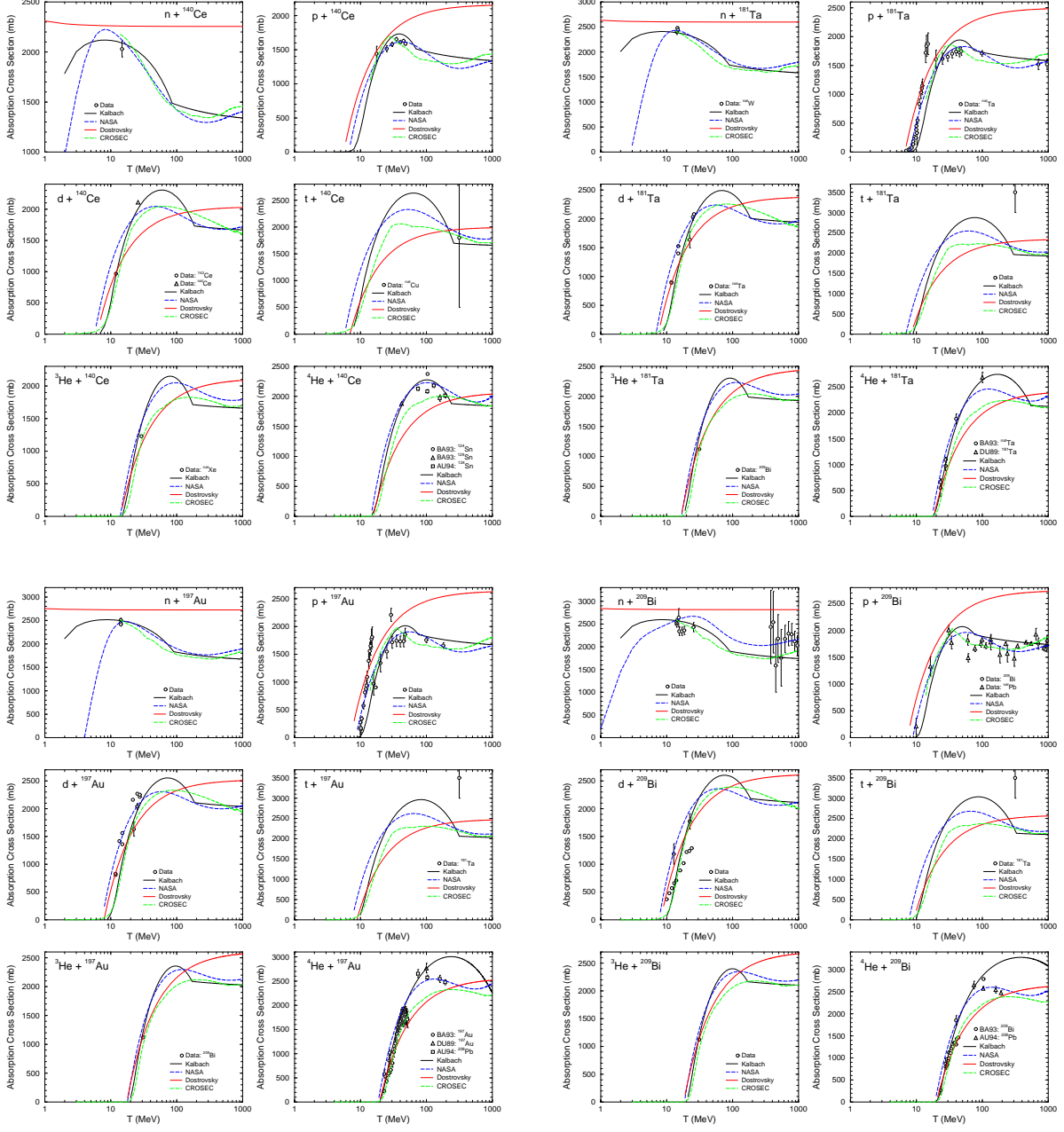


FIG. 11. Examples of total reaction cross section on target-nuclei ^{140}Ce , ^{181}Ta , ^{197}Au , and ^{209}Bi studied in Refs. [32, 33] with Kalbach [12], NASA [4–6], Tsang *et al.* [11], Dostrovsky *et al.* [3], and Barashenkov and Polansky (CROSEC) [13] systematics compared with experimental data (references on experimental data can be found in [32]).

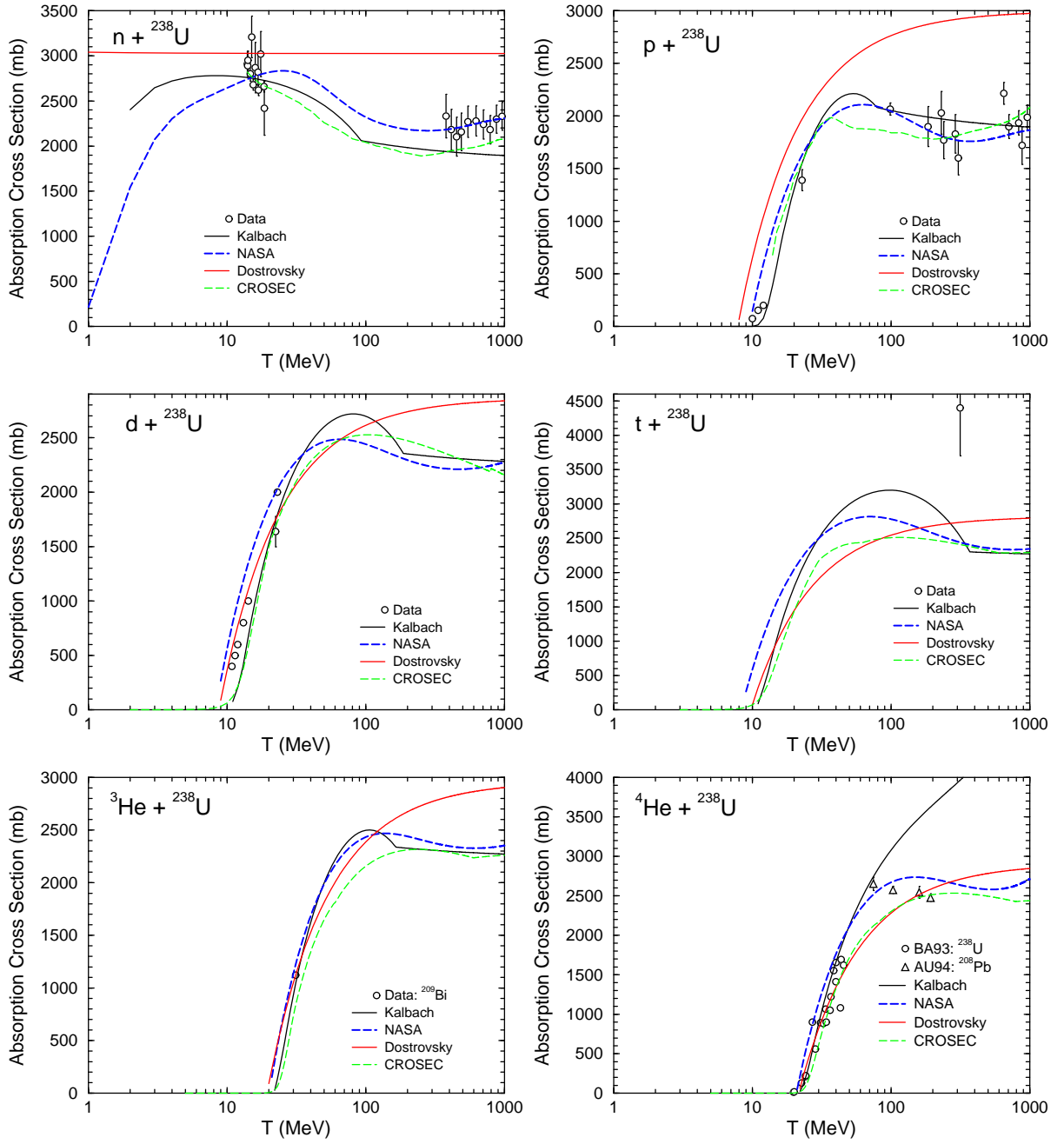


FIG. 12. Examples of total reaction cross section on target-nuclei ^{238}U studied in Refs. [32, 33] with Kalbach [12], NASA [4–6], Tsang *et al.* [11], Dostrovsky *et al.* [3], and Barashenkov and Polansky (CROSEC) [13] systematics compared with experimental data (references on experimental data can be found in [32]).

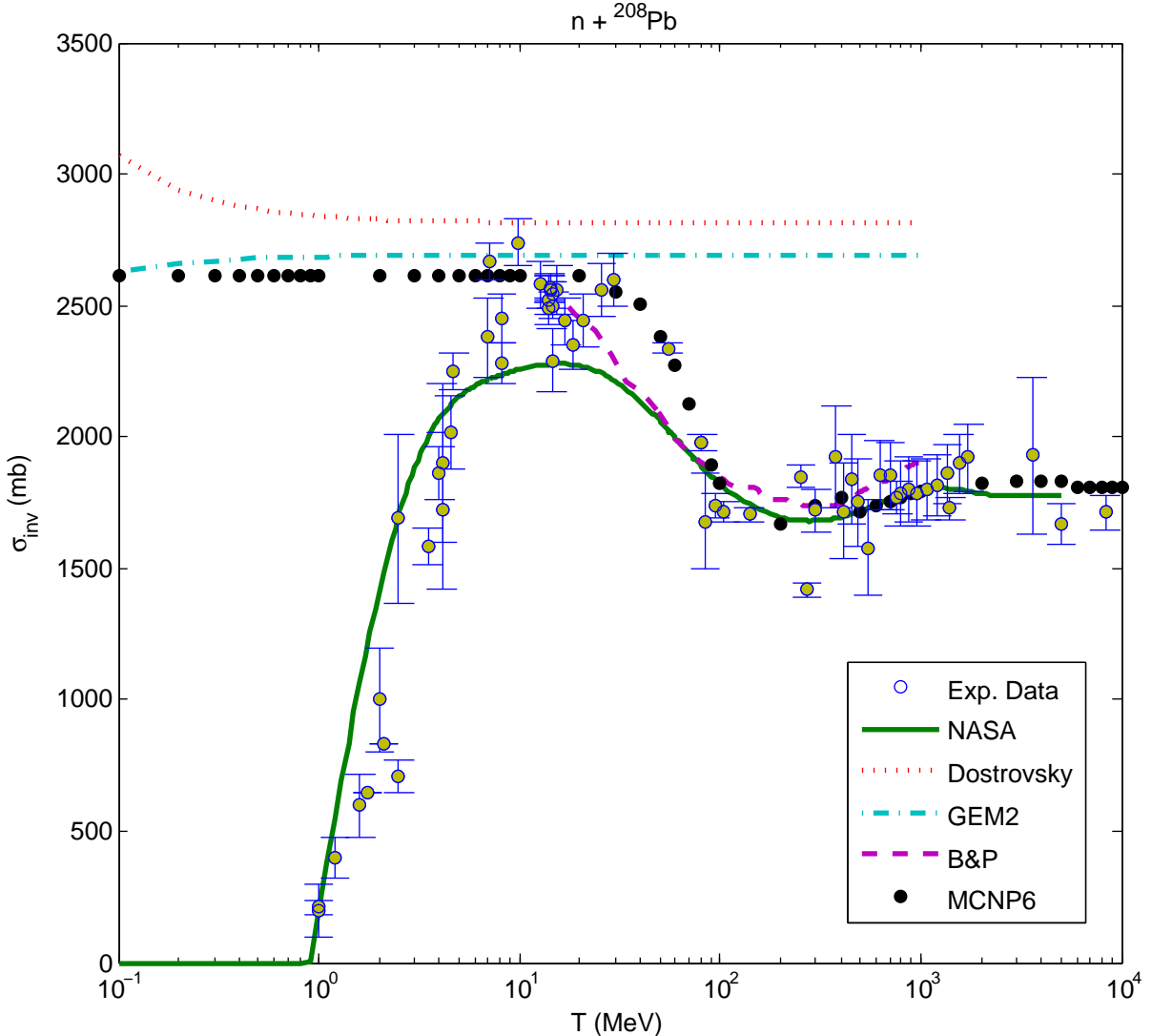


FIG. 13. Reaction cross section for $n + {}^{208}\text{Pb}$, as calculated by the NASA, Dostrovsky, GEM2, and B&P models. The black dots are cross section calculations of MCNP6, and the yellow points are experimental data [35–45].

B. Proton-Induced Reactions

Fig. 15 illustrates calculated cross sections by the NASA, Dostrovsky, GEM2, and B&P models, compared to calculations by MCNP6 and experimental data. The NASA model appears to be superior to the Dostrovsky-based models.

Fig. 16 displays the total reaction cross section for $p + {}^{28}\text{Si}$, ${}^{56}\text{Fe}$, ${}^{107}\text{Ag}$, and ${}^{197}\text{Au}$, as calculated by the NASA, Dostrovsky, and GEM2 models and compared to experimental

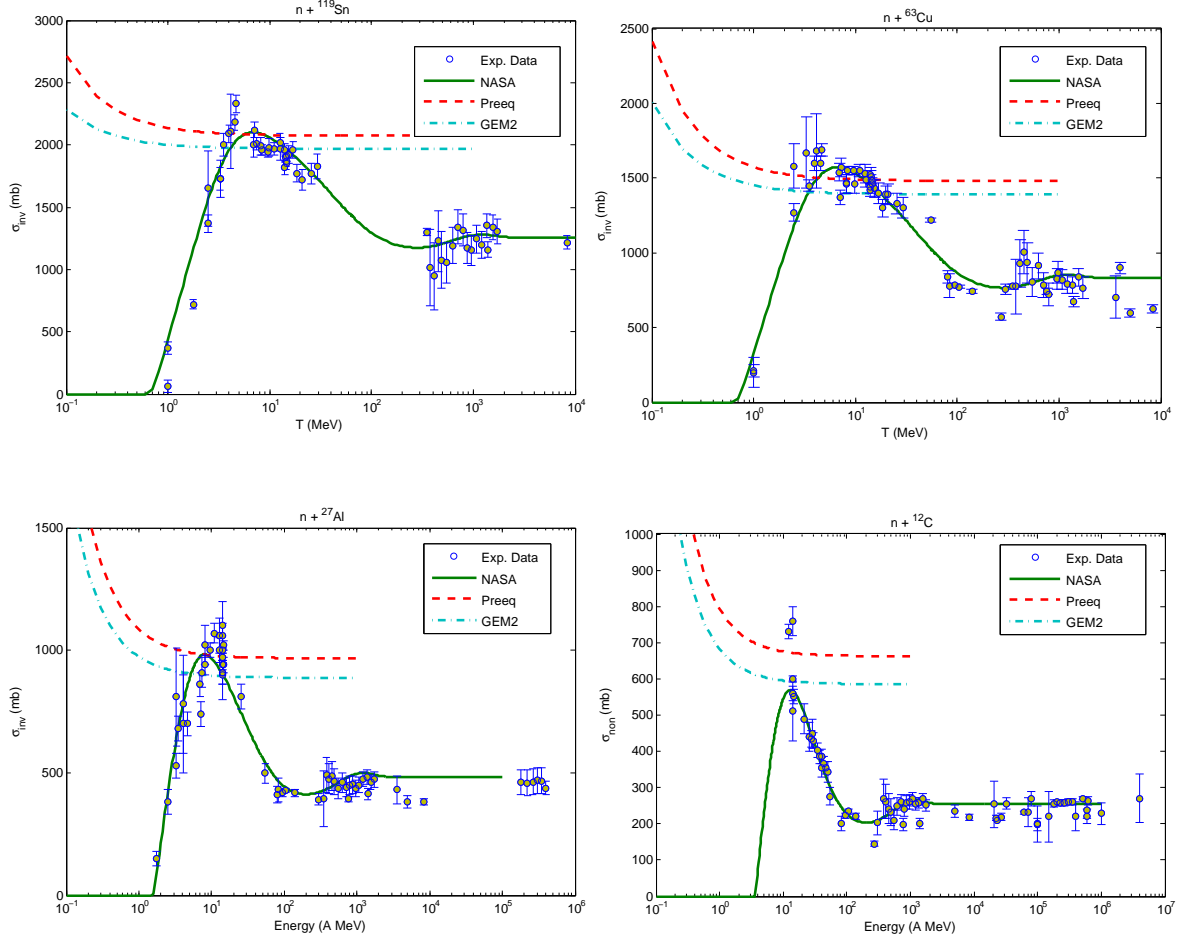


FIG. 14. Reaction cross section for various neutron-induced reactions, as calculated by the NASA, Dostrovsky, and GEM2 models. The yellow points are experimental data [35–39, 46–48].

data.

C. Heavy-Ion Induced Reactions

We never tested before how CEM03.03 calculates inverse cross sections for light fragments (LF) heavier than ${}^4\text{He}$. We address this question below.

Fig. 17 illustrates calculated cross sections by the NASA, Dostrovsky, GEM2, and B&P models for the reactions $\alpha + {}^{28}\text{Si}$ and ${}^6\text{Li} + {}^{208}\text{Pb}$, compared to experimental data.

Fig. 18 displays the total reaction cross section for ${}^4\text{He} + {}^{208}\text{Pb}$, ${}^4\text{He} + {}^{238}\text{U}$, ${}^6\text{He} + {}^{28}\text{Si}$, ${}^6\text{He} + {}^{63}\text{Cu}$, ${}^6\text{Li} + {}^{28}\text{Si}$, and ${}^6\text{Li} + {}^{90}\text{Zr}$, as calculated by the NASA, Dostrovsky, GEM2,

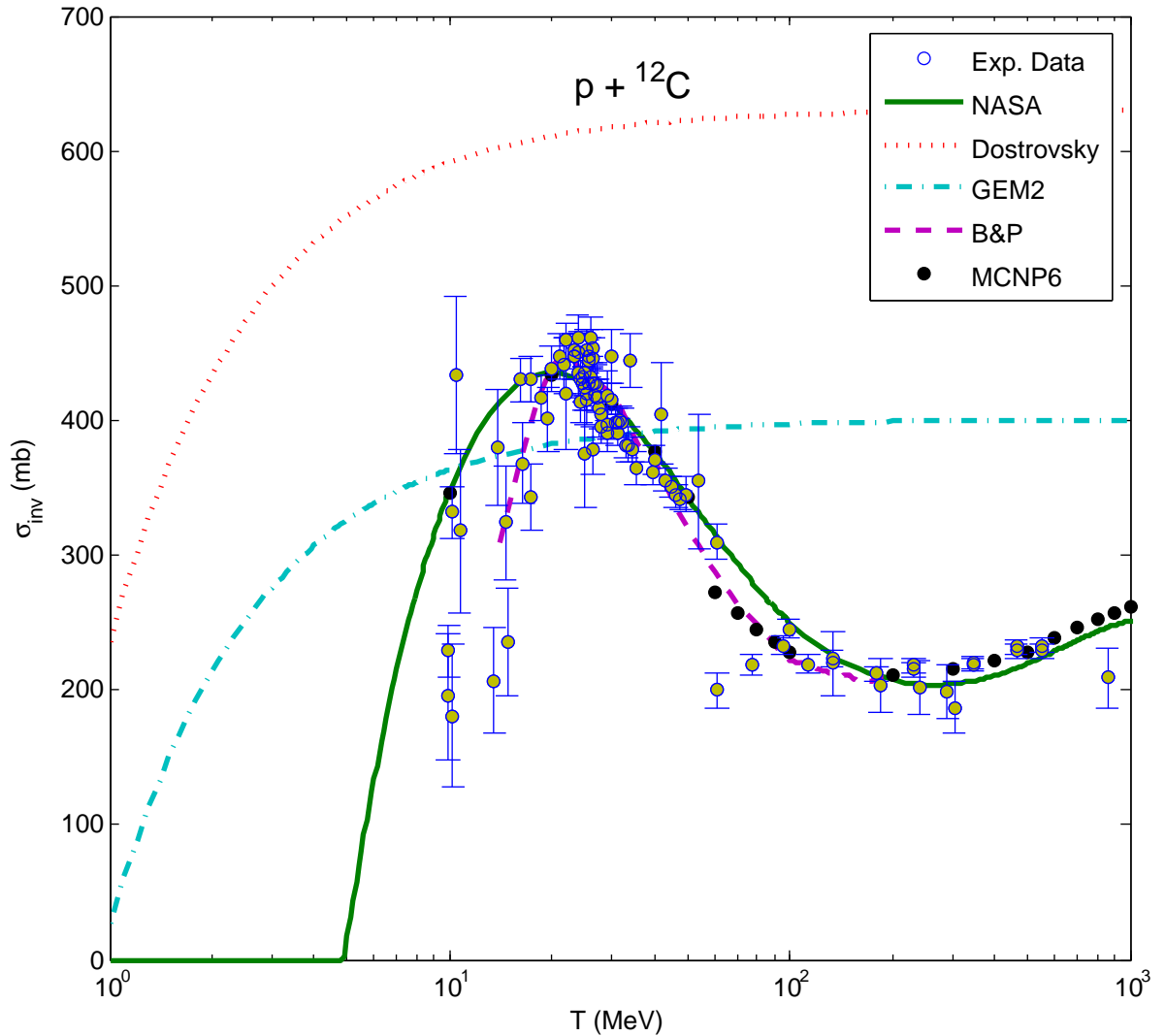


FIG. 15. Reaction cross section for $p + {}^{12}\text{C}$, as calculated by the NASA, Dostrovsky, GEM2, and B&P models. The black dots are cross section calculations of MCNP6, and the yellow points are experimental data [49].

and B&P models and compared to experimental data.

Fig. 19 displays the total reaction cross section for ${}^7\text{Be} + {}^{28}\text{Si}$, ${}^7\text{Li} + {}^{28}\text{Si}$, ${}^7\text{Li} + {}^{208}\text{Pb}$, ${}^8\text{He} + {}^{28}\text{Si}$, ${}^{10}\text{B} + {}^{28}\text{Si}$, and ${}^{10}\text{Be} + {}^{208}\text{Pb}$, as calculated by the NASA, Dostrovsky, GEM2, and B&P models and compared to experimental data.

Fig. 20 displays the total reaction cross section for ${}^{11}\text{Be} + {}^{208}\text{Pb}$ and ${}^{11}\text{C} + {}^{28}\text{Si}$, as calculated by the NASA, Dostrovsky, GEM2, and B&P models and compared to experimental

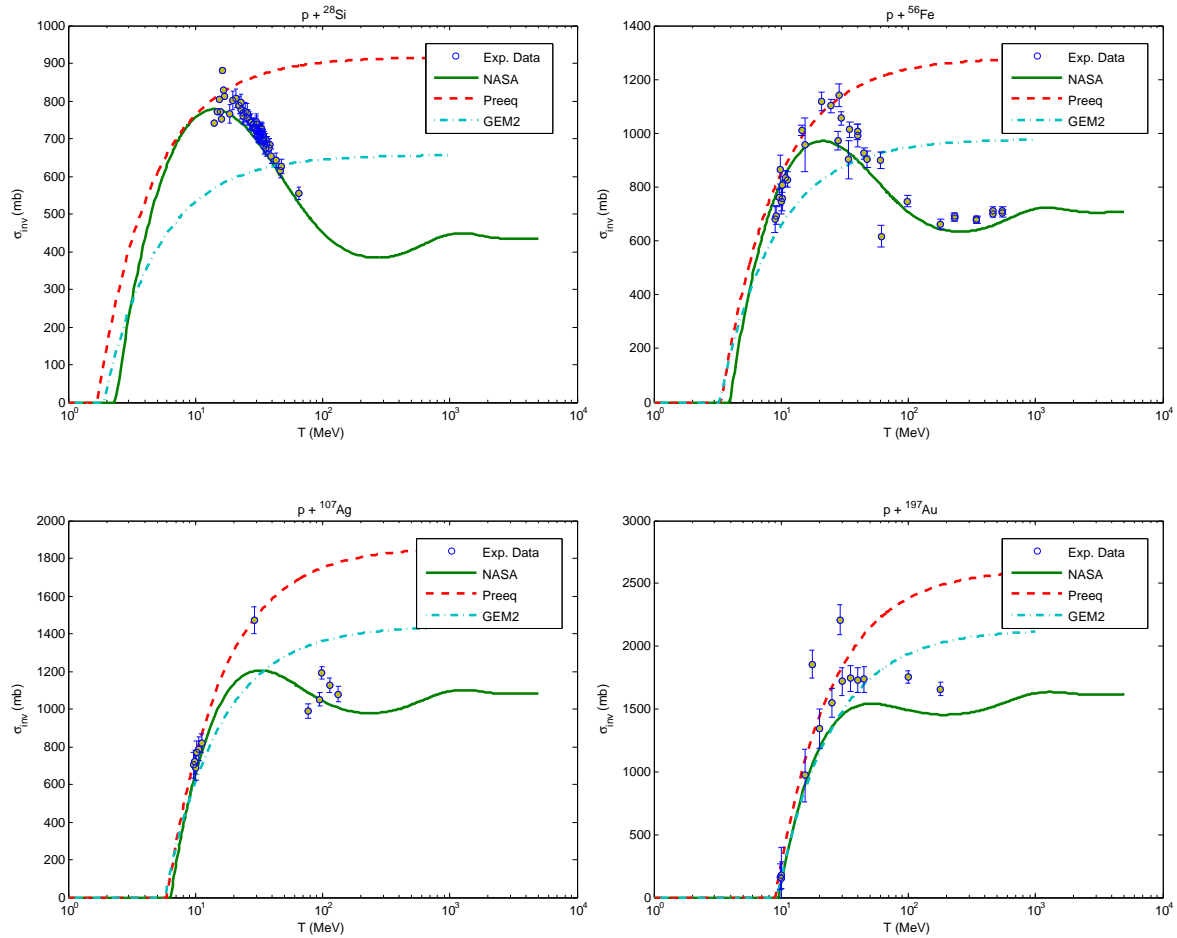


FIG. 16. Reaction cross section for various proton-induced reactions, as calculated by the NASA, Dostrovsky, and GEM2 models. The yellow points are experimental data [49–51].

data.

Fig. 21 displays the total reaction cross section for $^{12}\text{C} + ^{12}\text{C}$, as calculated by the NASA, Dostrovsky, GEM2, and B&P models and compared to experimental data and to measured total charge-changing (TCC) cross sections. TCC cross sections should be 5% – 10% less than total reaction cross sections, as TCC cross sections do not include the neutron removal cross section.

The NASA (Tripathi) cross section model seems to fit the experimentally measured data, in general, better than the other models tested.

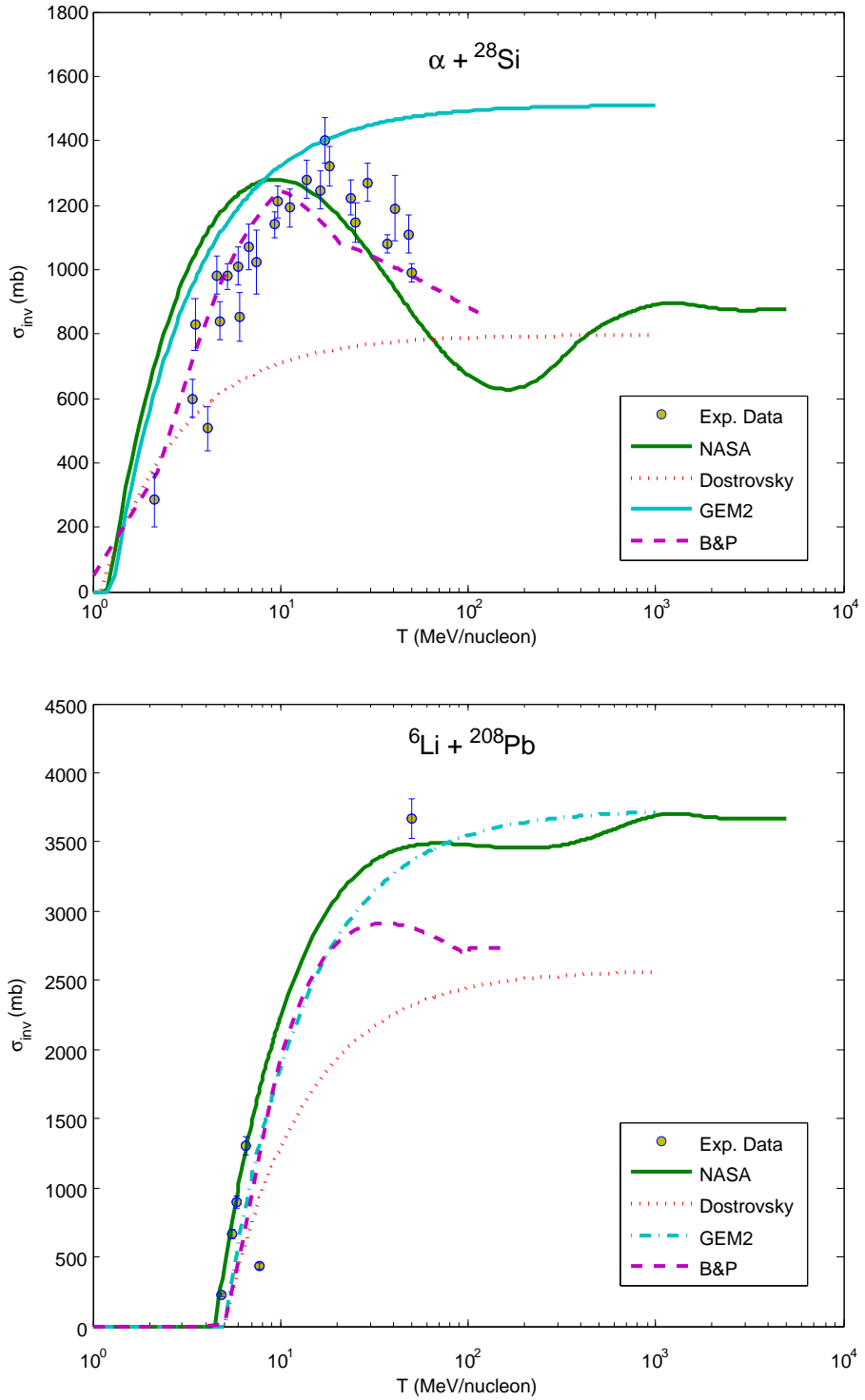


FIG. 17. Reaction cross section for $\alpha + {}^{28}\text{Si}$ and ${}^6\text{Li} + {}^{208}\text{Pb}$, as calculated by the NASA, Dostrovsky, GEM2, and B&P models. The yellow points are experimental data [52–56].

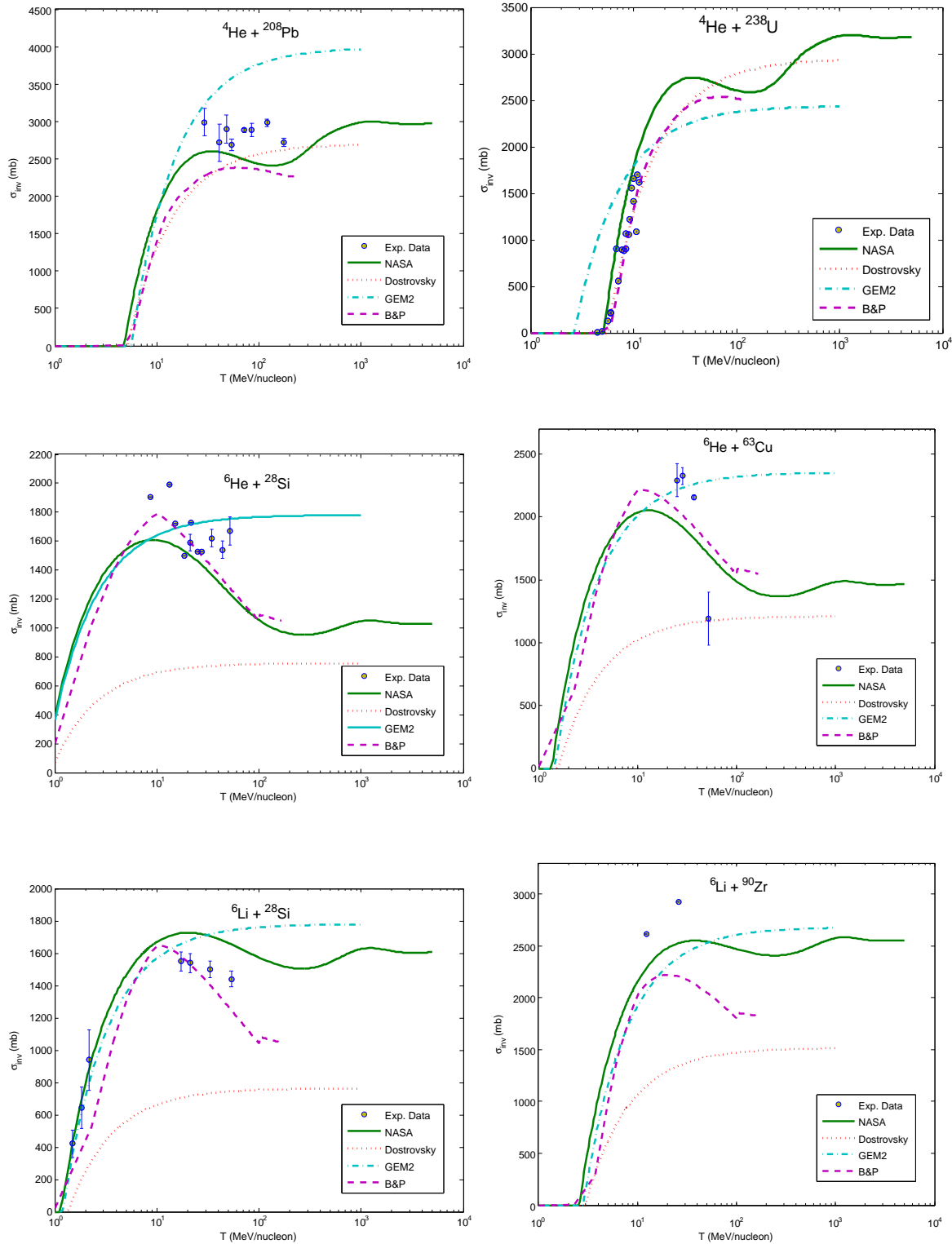


FIG. 18. Reaction cross section for various heavy-ion-induced reactions, as calculated by the NASA, Dostrovsky, GEM2, and B&P models. The yellow points are experimental data [57–59].

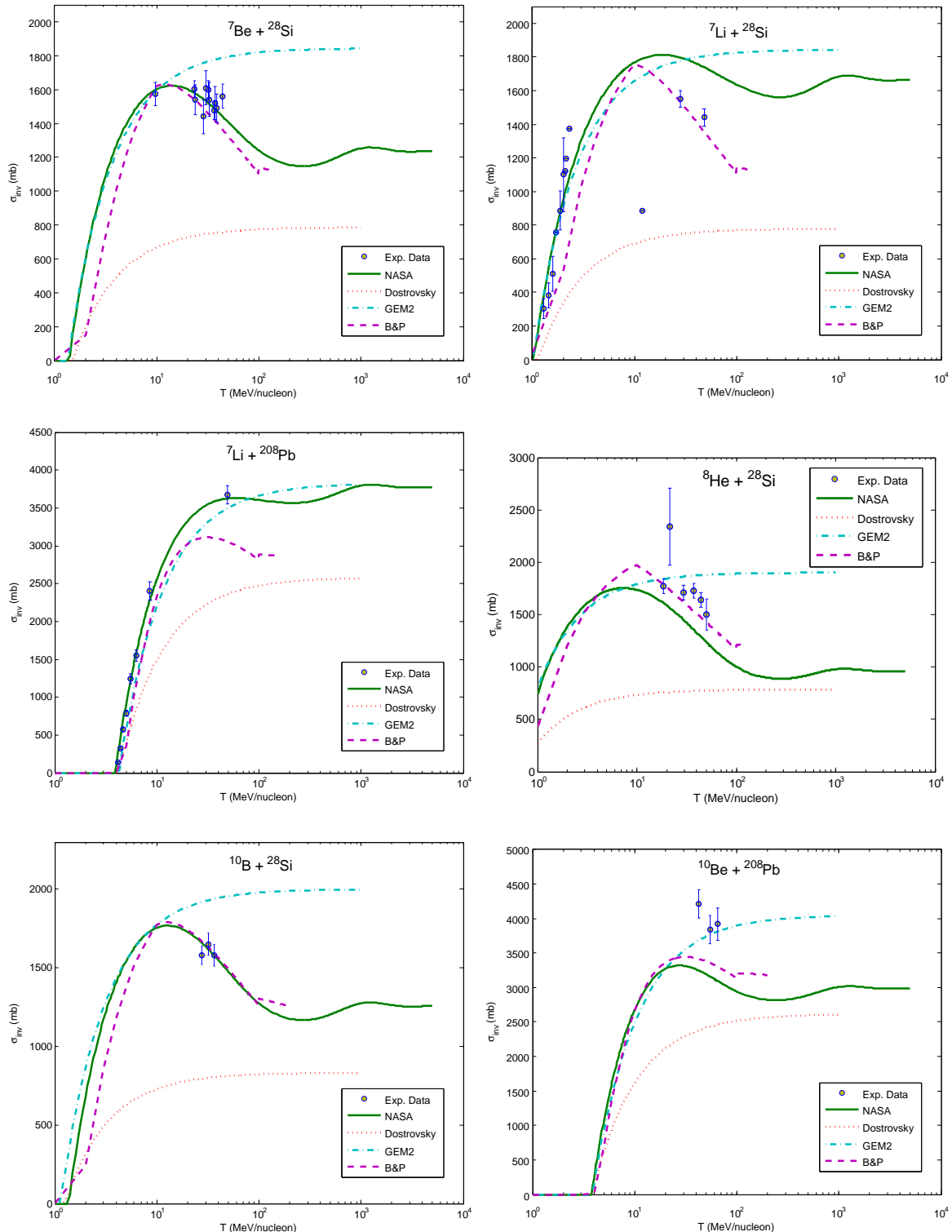


FIG. 19. Reaction cross section for various heavy-ion-induced reactions, as calculated by the NASA, Dostrovsky, GEM2, and B&P models. The yellow points are experimental data [52, 57, 60–65].

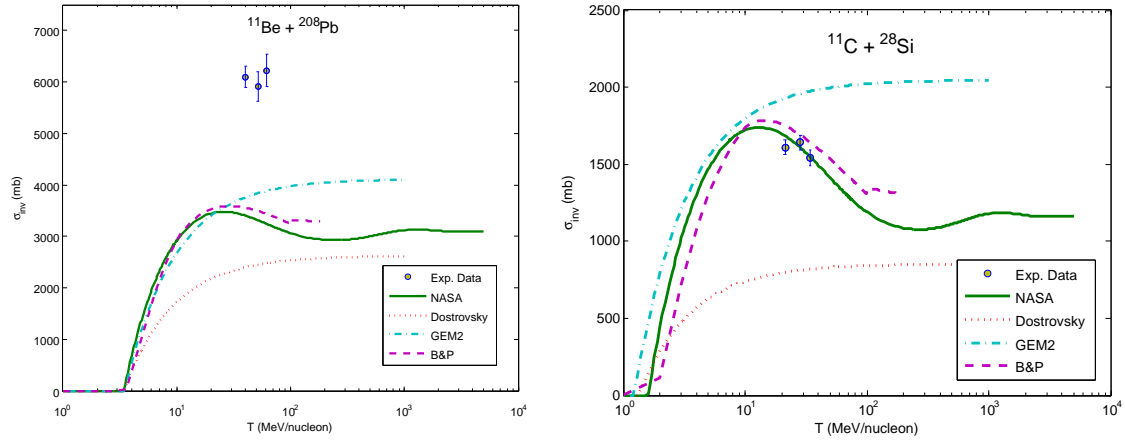


FIG. 20. Reaction cross section for various heavy-ion-induced reactions, as calculated by the NASA, Dostrovsky, GEM2, and B&P models. The yellow points are experimental data [61, 62].

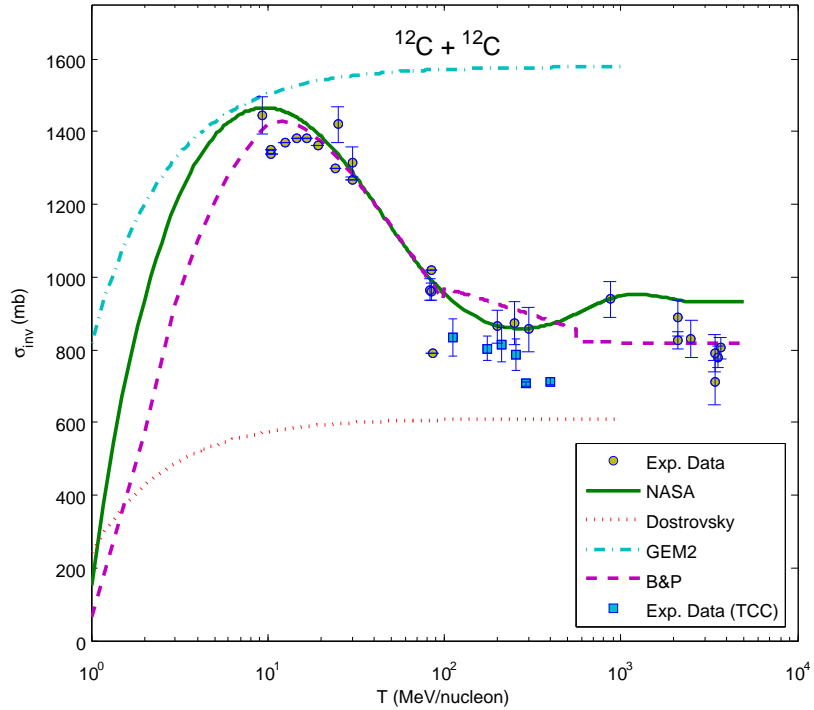


FIG. 21. Reaction cross section for various heavy-ion-induced reactions, as calculated by the NASA, Dostrovsky, GEM2, and B&P models. The yellow points are experimental data [48, 66] and the blue squares are total charge-changing cross section (TCC) measurements [67, 68].

VI. IMPLEMENTATION OF NASA CROSS SECTION MODEL INTO MEM

A. Emission Width, Γ_j , Calculation

CEM uses the inverse cross section, σ_{inv} , in determining what particles and/or fragments are emitted from the excited nucleus. The probability of emitting fragment type j , called the emission width Γ_j , is calculated according to Eq. 3, and is dependent upon σ_{inv} .

$$\Gamma_j(p, h, E) = \int_{V_j^c}^{E-B_j} \gamma_j \frac{2s_j + 1}{\pi^2 \hbar^3} \mu_j \Re(p, h) \frac{\omega(p - 1, h, E - B_j - T)}{\omega(p, h, E)} T \sigma_{inv}(T) dT, \quad (3)$$

where:

p is number of particle excitons;

h is number of hole excitons;

E is internal energy of the excited nucleus (sometimes referred to as U);

B_j is the binding energy of particle j ;

V_j^c is Coulomb barrier of particle j ;

γ_j is probability that the proper number of particle excitons will coalesce to form a type j fragment (also called γ_β in a number of early publications; see, *e.g.*, Refs. [69, 70]);

s_j is the spin of the emitted particle j ;

μ_j is the reduced mass of the emitted particle j ;

\Re creates zero probability of emission if the number of particle excitons is less than the number of nucleons in particle j ;

ω is the level density of the n -exciton state;

T is the kinetic energy of the emitted particle j ;

σ_{inv} is the inverse cross section.

In the old calculation by CEM03.03 (called `gamagu2`), the Dostrovsky form of the cross section was simple enough that for neutrons and protons this integral could be evaluated analytically. However, for complex particles the level density (or ω) becomes too complicated and the integral is evaluated numerically. In this case a 6-point Gaussian quadrature was used when the exciton number is 15 or less, and a 6-point Gauss-Laguerre quadrature was used when the number of excitons is over 15. We will see later why the two methods are needed.

In the new calculation we adopt here for CEM03.03F (called `gamagu3`), the NASA form of the cross section is too complicated and the integral is always calculated numerically. We started by using an 8-point Gaussian quadrature.

For a little bit of history, there was a `gamagu` “the first,” of this series (actually, the very first FORTRAN function to calculate Γ_j in the MEM code MODEX [30] was called `gammap`; later, several updates and improvements were used in MEM under a name of `gammam`, until `gamagu` was introduced in an early version of CEM). This was similar to `gamagu3`. In other words, it used 8-point Gaussian quadrature and accepted a general form for the inverse cross section. And then about ten years ago Arnold Sierk upgraded it to include 1) analytical integration for nucleons and 2) Gauss-Laguerre quadrature for high exciton number. While this was an improvement, in this process the Dostrovsky cross section was “hard-wired” into the Γ_j calculation, so that when we began this project, we started with the older Γ_j calculation (`gamagu`), before it had been modified, as it allows for a general form for the inverse cross section.

Fig. 22 shows the plots of Γ_j as a function of the internal energy of the excited nucleus for emitted protons and ^4He from an excited ^{198}Au nucleus with 55 excitons, 25 particle excitons, and 13 charged particle excitons. Remember that these are unnormalized probabilities of emission. Gamagu2 is the old CEM03.03 Γ_j calculation. Gamagu3 is the new calculation, using either the Dostrovsky or NASA cross section. Gamagu2 should be very similar to Gamagu3-Dostrovsky because the only significant difference is the method of integration. For protons this difference is roughly 15%, for α it is not significant. Protons are calculated analytically in `gamagu2`, and with an 8-pt Gaussian quadrature in `gamagu3`. From our tests, changing from a 6-point to an 8-point Gaussian quadrature can make as much as a 25% difference, and changing from the Gauss-Legendre to a Gauss-Laguerre can make as much as a 35% difference. This is a clue that the numerical integration needed to be re-evaluated, which we detail in a subsequent section.

Fig. 23 plots Γ_j for ^6Li , for the same excited ^{198}Au nucleus. Note that the old `gamagu2` was hard-wired to only work properly for up to ^4He . This is because of how it calculated this term here:

$$\left(\frac{T + Bj}{E} \right)^{A_j - 1.5}. \quad (4)$$

Instead of putting in the A-number of the fragment considered into Eq. 4, it used IF statements to decide if the emitted fragment was a deuteron, triton, ^3He , or ^4He , and

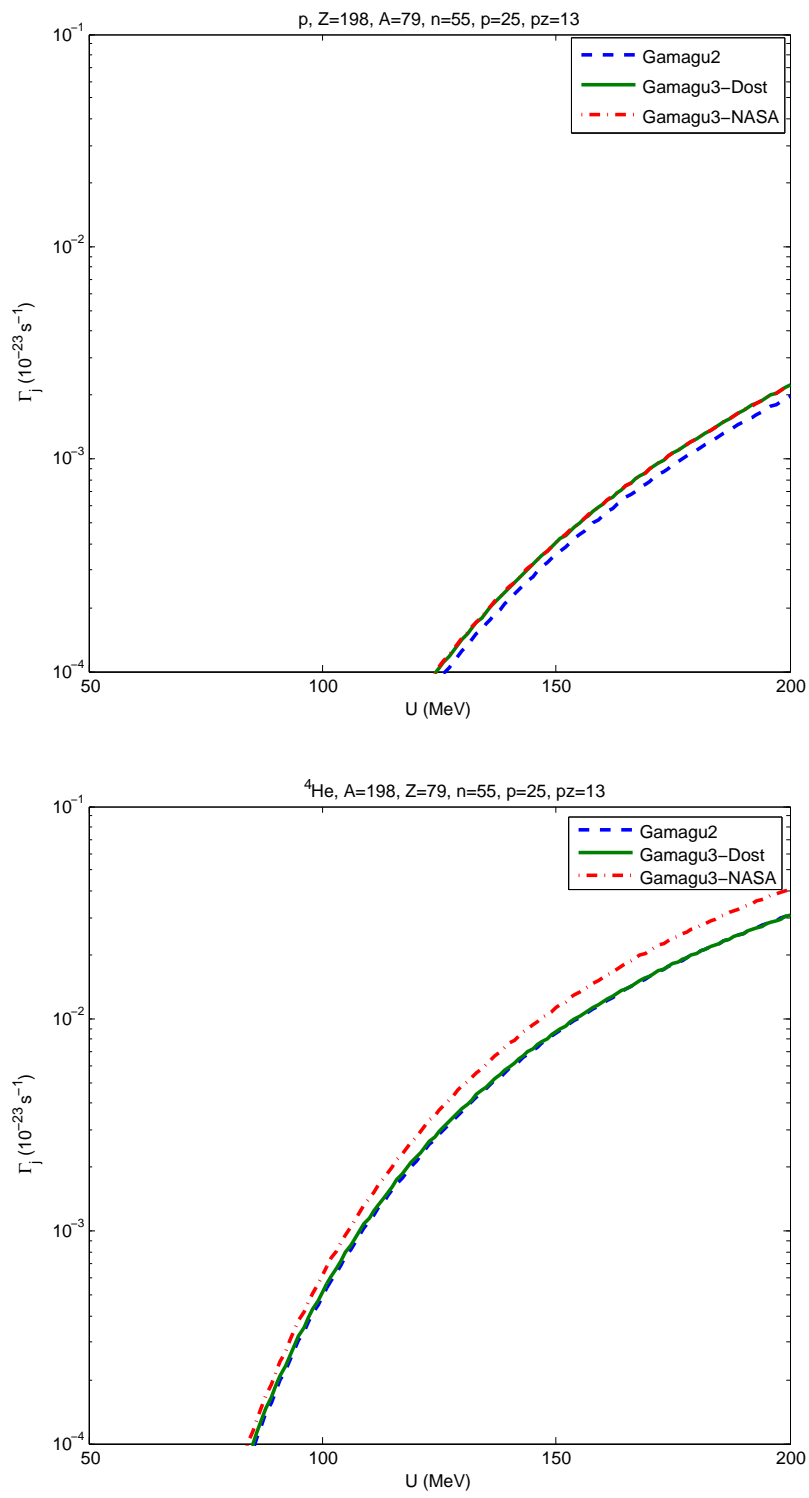


FIG. 22. Γ_j as a function of the internal energy of the excited nucleus for emitted protons and ^4He from an excited ^{198}Au nucleus with 55 excitons, 25 particle excitons, and 13 charged particle excitons.

multiply by the factor $((T + Bj)/E)$ the correct number of times. So for fragments larger than ${}^4\text{He}$ it does not work. This does not effect the old CEM03.03 results at all, as CEM03.03 does not allow for the emission of anything heavier than ${}^4\text{He}$ in its MEM anyway. This will, however, significantly impact our γ_j parameterization for our expanded MEM. Referring to Eq. 3, the lowercase γ_j (also often called γ_β) is a measure of the probability of the particle excitons to coalesce and form a light fragment. However, this is too computationally time-consuming to calculate accurately for complex particles and so is approximated and then adjusted to match experimental data, as was done in the past by other authors (see, *e.g.*, Refs. [69, 70]).

Fig. 24 shows Γ_j for neutrons for the same ${}^{198}\text{Au}$ excited nucleus. Remember that the NASA cross section goes to zero for low-energy neutrons, making it unsuitable for an inverse neutron cross section calculation without modification. We need to implement Kalbach systematics into our NASA cross section, for low-energy neutrons, which we have done and show our results in the next section. However, upon further investigation we also discovered

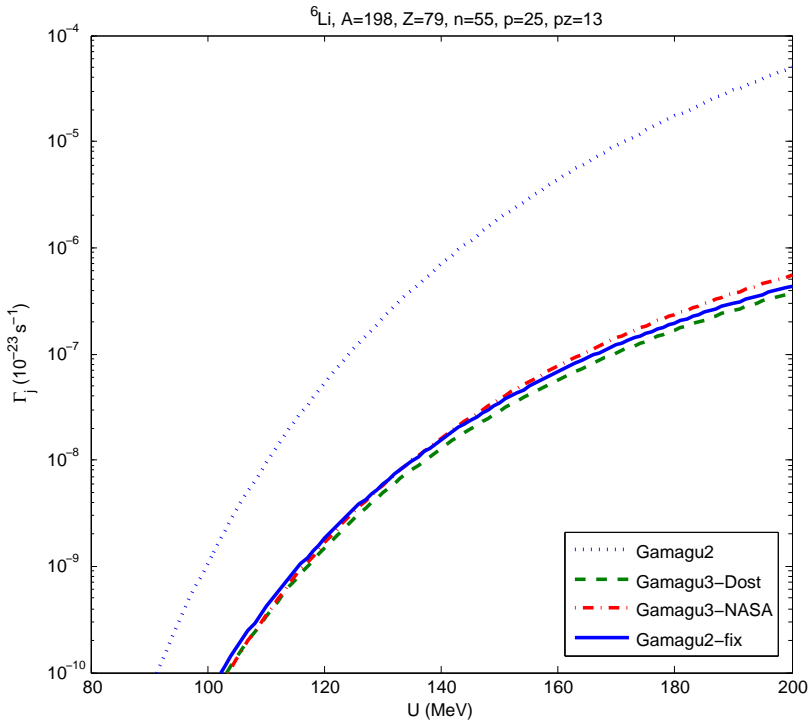


FIG. 23. Γ_j as a function of the internal energy of the excited nucleus for emitted ${}^6\text{Li}$ from an excited ${}^{198}\text{Au}$ nucleus with 55 excitons, 25 particle excitons, and 13 charged particle excitons.

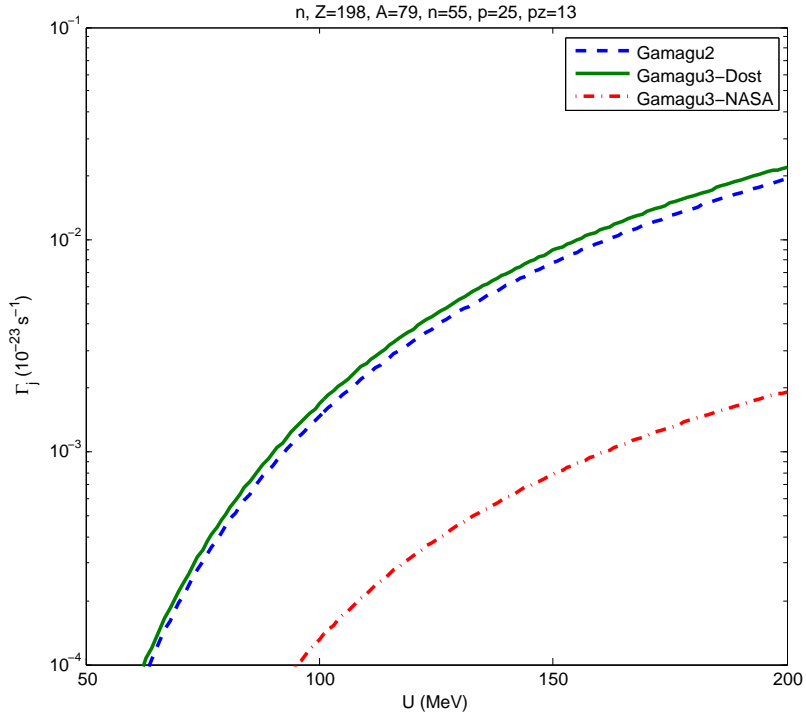


FIG. 24. Γ_j as a function of the internal energy of the excited nucleus for emitted neutrons from an excited ^{198}Au nucleus with 55 excitons, 25 particle excitons, and 13 charged particle excitons.

the issue is exacerbated by our initial integration method (8-pt Gaussian quadrature only).

Fig. 25 is a snapshot of the integrand, λ_j , the partial transmission probability, or the probability that fragment type j will be emitted with kinetic energy T . This λ_j is for the emission of neutrons from the same ^{198}Au excited nucleus as before, with an internal nucleus energy of 200 MeV. Our Gaussian quadrature will be sampling from 0 to roughly 200 MeV, however λ_j becomes negligible by about 40 MeV. Table I displays the abscissas for an 8-point Gauss-Legendre and an 8-point Gauss-Laguerre quadrature. What is interesting to note is that with the NASA cross section, the 8-pt Gaussian quadrature almost entirely misses the peak (as there are samples taken at $T=3.84$ and 19.7 MeV). Thus the very low values of Γ_n .

However, in this case we have 55 excitons—quite a large number—and one that would in the old calculation integrate by the 6-point Gauss-Laguerre method (if it wasn't done analytically). This method has much better sampling points for this case. For cases of low exciton number, the peak becomes increasingly spread out (see Fig. 26 for an example of 10 excitons), and so the simple Gaussian performs adequately.

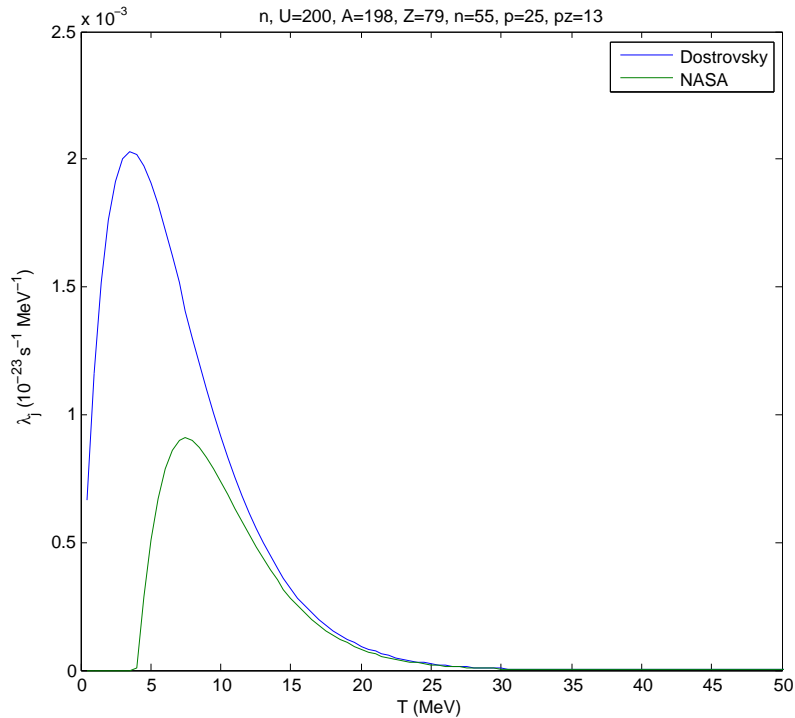


FIG. 25. λ_j as a function of the kinetic energy of the emitted neutron, from an excited ^{198}Au nucleus with $U = 200$ MeV and 55 excitons, 25 particle excitons, and 13 charged particle excitons.

TABLE I. 8-point Gaussian and Gauss-Laguerre sampling points

8-pt Gaussian		8-pt Gauss-Laguerre	
3.84 MeV		0.428 MeV	
19.7 MeV		2.27 MeV	
45.9 MeV		5.66 MeV	
79.0 MeV		10.7 MeV	
114. MeV		17.7 MeV	
148. MeV		27.1 MeV	
174. MeV		39.6 MeV	
190. MeV		57.5 MeV	

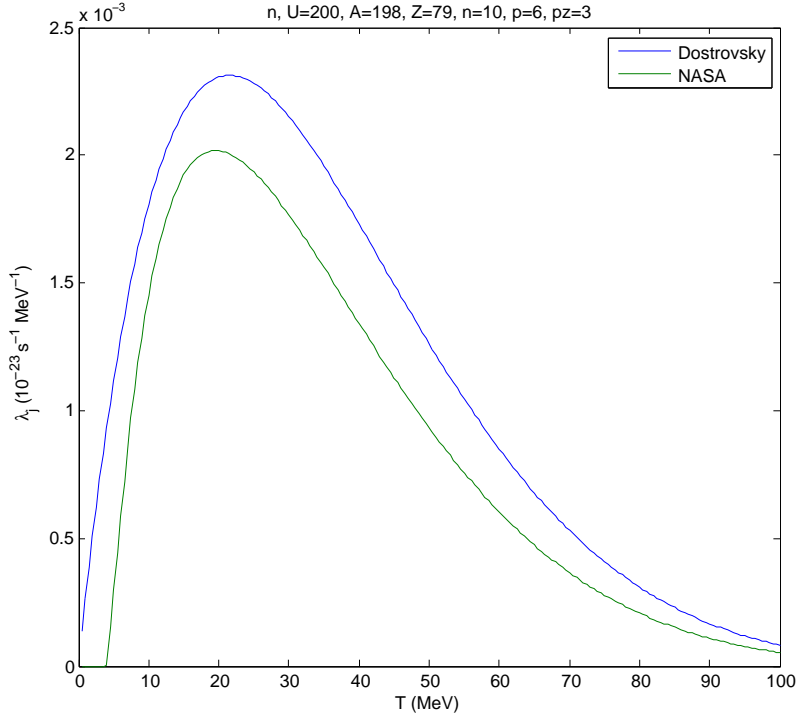


FIG. 26. λ_j as a function of the kinetic energy of the emitted neutron, from an excited ^{198}Au nucleus with $U = 200$ MeV and 10 excitons, 6 particle excitons, and 3 charged particle excitons.

B. Kalbach Systematics

We added Kalbach systematics to fix the NASA cross section for low-energy neutrons. Fig. 27 displays the Kalbach implementation for the cross section $n + ^{208}\text{Pb}$. At around 24 MeV and below the calculation switches to Kalbach, and is NASA throughout the rest of the spectrum. The Kalbach is scaled to match the NASA at the switchpoint so as not to have a large jump. Fig. 28 shows our new Γ_n . It is much improved, as expected.

As part of the Kalbach implementation, switchpoints and scaling factors must be obtained for all possible residual nuclei, by mass number. Table II lists these switchpoints and scaling factors calculated in this work, so as to maintain a smooth cross section energy dependence.

TABLE II: Switchpoints and scaling factors for the Kalbach implementation

A_{residual}	Switchpoint (MeV)	Scaling Factor	A_{residual}	Switchpoint (MeV)	Scaling Factor
2	14.55	0.00	3	14.97	0.6757
Continued on next page					

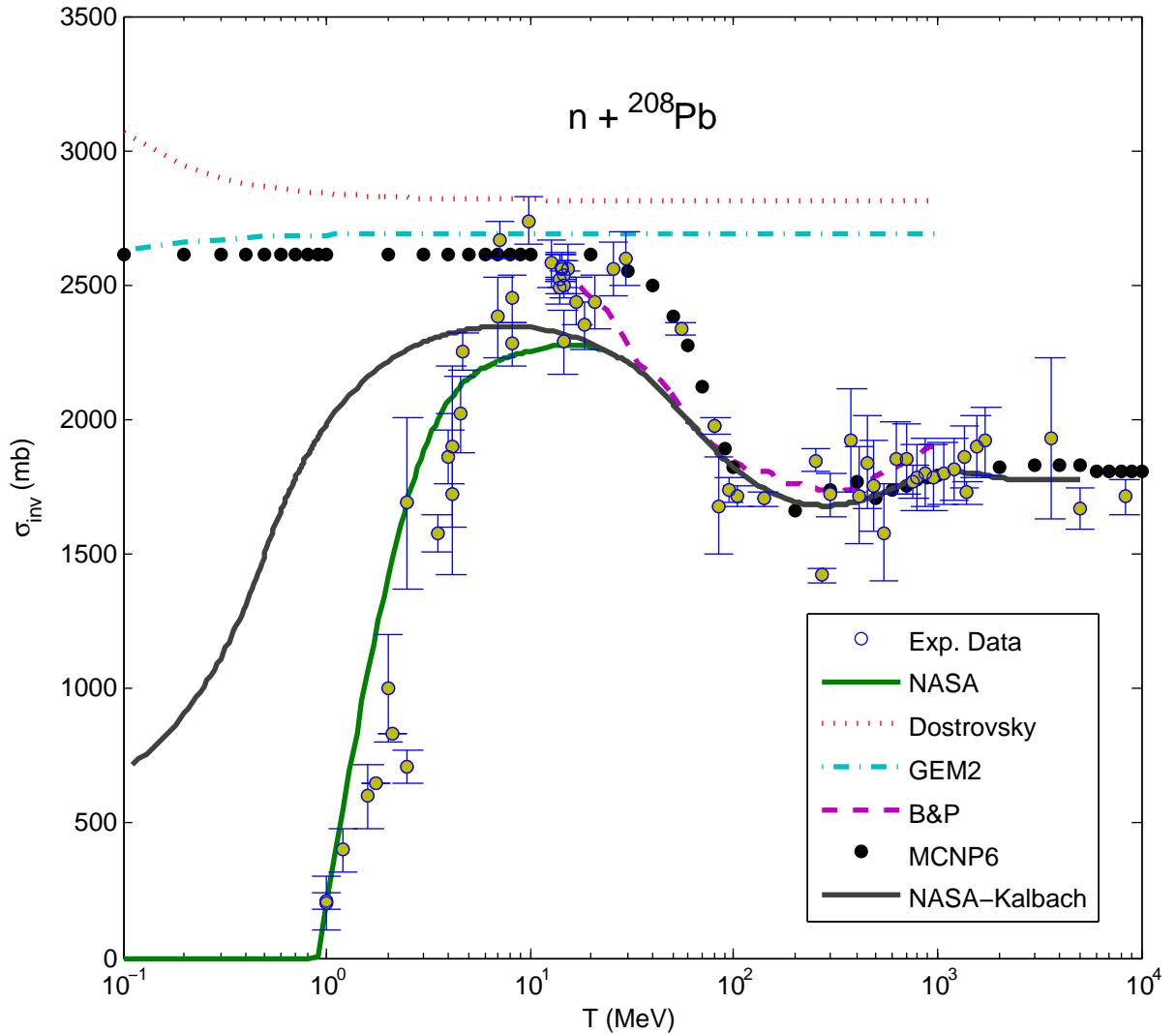


FIG. 27. Reaction cross section for $n + {}^{208}\text{Pb}$, as calculated by the NASA, NASA-Kalbach hybrid, Dostrovsky, GEM2, and B&P models. The black dots are cross section calculations of MCNP6, and the yellow points are experimental data [35–45].

TABLE II – continued from previous page

A_{residual}	Switchpoint (MeV)	Scaling Factor	A_{residual}	Switchpoint (MeV)	Scaling Factor
4	55.64	0.5922	5	6.32	1.111
6	6.30	1.057	7	6.24	1.099
8	6.46	1.144	9	6.24	1.122

Continued on next page

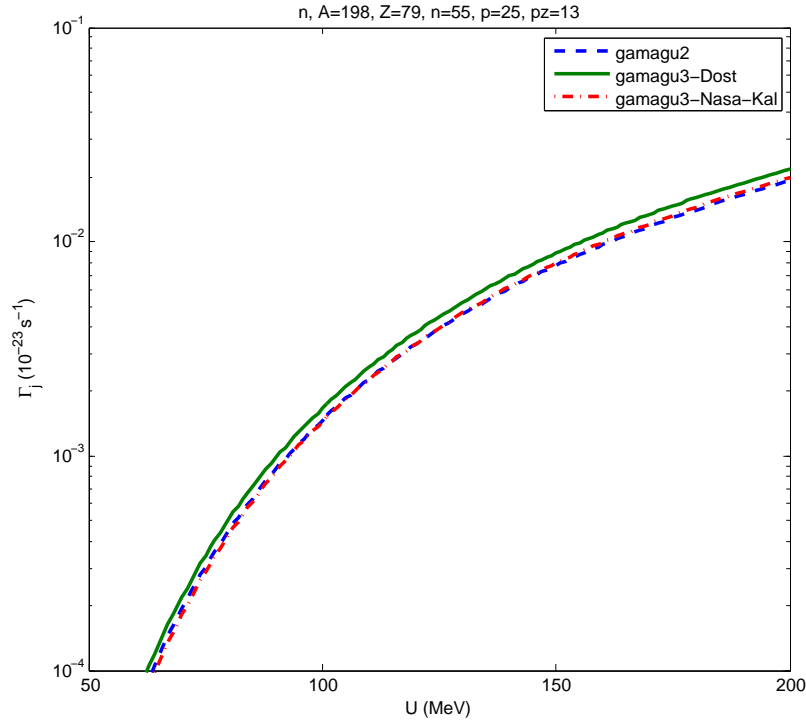


FIG. 28. Γ_j as a function of the internal energy of the excited nucleus for emitted neutrons from an excited ^{198}Au nucleus with 55 excitons, 25 particle excitons, and 13 charged particle excitons.

TABLE II – continued from previous page

$A_{residual}$	Switchpoint (MeV)	Scaling Factor	$A_{residual}$	Switchpoint (MeV)	Scaling Factor
10	6.36	1.13	11	5.95	1.089
12	12.94	0.9642	13	8.86	1.062
14	8.85	1.045	15	8.70	1.055
16	8.69	1.04	17	8.63	1.050
18	8.64	1.059	19	9.03	1.047
20	8.99	1.031	21	9.01	1.040
22	8.97	1.05	23	8.87	1.038
24	8.80	1.026	25	8.66	1.031
26	8.72	1.037	27	8.82	1.028
28	8.81	1.016	29	8.47	1.017

Continued on next page

TABLE II – continued from previous page

$A_{residual}$	Switchpoint (MeV)	Scaling Factor	$A_{residual}$	Switchpoint (MeV)	Scaling Factor
30	8.47	1.019	31	8.34	1.008
32	8.33	0.9962	33	8.21	0.9965
34	8.20	0.9967	35	8.08	0.9851
36	8.07	0.9856	37	7.96	0.9841
38	7.94	0.9812	39	7.83	0.9680
40	8.15	0.9675	41	8.75	1.028
42	8.61	1.031	43	8.59	1.034
44	8.47	1.037	45	8.43	1.040
46	8.41	1.043	47	8.30	1.046
48	8.27	1.048	49	8.17	1.050
50	8.14	1.052	51	8.09	1.054
52	7.32	1.049	53	7.29	1.051
54	7.21	1.052	55	7.17	1.054
56	7.15	1.055	57	7.07	1.056
58	7.05	1.057	59	6.97	1.058
60	6.71	1.051	61	6.67	1.052
62	6.63	1.053	63	6.59	1.054
64	6.23	1.054	65	6.20	1.055
66	6.17	1.055	67	6.46	1.058
68	6.42	1.059	69	6.40	1.061
70	6.38	1.061	71	6.34	1.062
72	6.32	1.063	73	6.30	1.064
74	6.28	1.065	75	6.25	1.066
76	6.24	1.066	77	6.22	1.067
78	6.21	1.068	79	6.19	1.068
80	6.17	1.069	81	6.17	1.070
82	6.16	1.070	83	6.15	1.071

Continued on next page

TABLE II – continued from previous page

$A_{residual}$	Switchpoint (MeV)	Scaling Factor	$A_{residual}$	Switchpoint (MeV)	Scaling Factor
84	6.14	1.071	85	6.14	1.072
86	6.13	1.073	87	6.12	1.073
88	6.12	1.074	89	6.12	1.074
90	6.12	1.074	91	6.11	1.074
92	6.12	1.074	93	6.14	1.074
94	6.14	1.074	95	6.15	1.074
96	6.16	1.074	97	6.19	1.074
98	6.18	1.074	99	6.21	1.073
100	6.23	1.073	101	6.24	1.073
102	6.26	1.073	103	6.25	1.073
104	6.31	1.073	105	6.33	1.072
106	6.36	1.072	107	6.38	1.072
108	6.42	1.072	109	6.45	1.071
110	6.48	1.071	111	6.52	1.070
112	6.55	1.070	113	6.58	1.069
114	6.62	1.069	115	6.67	1.069
116	6.71	1.068	117	6.74	1.067
118	6.80	1.067	119	6.85	1.066
120	6.89	1.066	121	6.95	1.065
122	7.00	1.064	123	7.05	1.064
124	7.10	1.063	125	7.16	1.063
126	7.21	1.062	127	7.28	1.061
128	7.33	1.060	129	7.40	1.060
130	7.46	1.059	131	7.53	1.058
132	7.60	1.057	133	7.68	1.056
134	7.74	1.055	135	7.82	1.054
136	7.89	1.053	137	7.97	1.052

Continued on next page

TABLE II – continued from previous page

$A_{residual}$	Switchpoint (MeV)	Scaling Factor	$A_{residual}$	Switchpoint (MeV)	Scaling Factor
138	8.04	1.051	139	8.12	1.050
140	8.21	1.048	141	8.59	1.047
142	8.67	1.046	143	8.78	1.045
144	8.85	1.044	145	8.96	1.042
146	9.06	1.041	147	9.13	1.033
148	9.25	1.039	149	9.33	1.037
150	9.46	1.036	151	9.57	1.035
152	9.66	1.033	153	9.77	1.031
154	9.87	1.030	155	9.98	1.029
156	10.12	1.028	157	10.22	1.026
158	10.34	1.025	159	10.47	1.027
160	10.55	1.022	161	10.71	1.021
162	10.83	1.020	163	10.96	1.018
164	11.08	1.017	165	11.22	1.017
166	11.31	1.015	167	11.47	1.013
168	11.63	1.012	169	11.75	1.012
170	11.90	1.009	171	12.06	1.008
172	12.16	1.007	173	12.35	1.005
174	12.48	1.004	175	12.64	1.002
176	12.80	1.002	177	12.94	0.9997
178	13.11	0.9992	179	13.25	0.9980
180	13.42	0.9968	181	13.60	0.9956
182	13.71	0.9944	183	13.91	0.9930
184	14.06	0.9920	185	14.23	0.9911
186	14.44	0.9899	187	14.60	0.9888
188	14.78	0.9868	189	14.96	0.9856
190	15.14	0.9845	191	15.31	0.9838

Continued on next page

TABLE II – continued from previous page

$A_{residual}$	Switchpoint (MeV)	Scaling Factor	$A_{residual}$	Switchpoint (MeV)	Scaling Factor
192	15.52	0.9827	193	15.70	0.9815
194	15.88	0.9799	195	16.10	0.9788
196	16.30	0.9776	197	16.47	0.9764
198	16.66	0.9752	199	16.86	0.9741
200	15.42	0.8902	201	15.45	0.8902
202	15.47	0.8903	203	15.53	0.8906
204	19.97	0.8992	205	19.98	0.8993
206	20.02	0.8990	207	25.02	0.9041
208	24.94	0.9042	209	25.06	0.9748
210	25.05	0.9740	211	25.02	0.9576
212	25.10	0.9585	213	25.05	0.9591
214	25.14	0.9600	215	25.10	0.9591
216	25.08	0.9583	217	25.16	0.9577
218	25.14	0.9571	219	25.20	0.9565
220	25.18	0.9704	221	25.15	0.9708
222	25.22	0.9701	223	25.21	0.9695
224	25.28	0.9689	225	25.27	0.9683
226	25.22	0.9544	227	25.29	0.9538
228	25.28	0.9532	229	25.33	0.9680
230	25.31	0.9672	231	25.29	0.9526
232	25.38	0.9660	233	25.34	0.9527
234	25.39	0.9661	235	25.38	0.9656
236	25.36	0.9647	237	25.44	0.9516
238	25.40	0.9638	239	25.47	0.9659
240	25.45	0.9652	241	25.43	0.9646
242	25.48	0.9522	243	25.45	0.9516
244	25.53	0.9511	245	25.50	0.9506

Continued on next page

TABLE II – continued from previous page

$A_{residual}$	Switchpoint (MeV)	Scaling Factor	$A_{residual}$	Switchpoint (MeV)	Scaling Factor
246	25.49	0.9500	247	25.55	0.9505
248	25.52	0.9510	249	25.58	0.9517
250	25.56	0.9522	251	25.55	0.9516
252	25.58	0.9511	253	25.58	0.9513
254	25.66	0.9520	255	25.63	0.9513
256	25.60	0.9507	257	25.66	0.9514
258	25.63	0.9518	259	25.68	0.9513
260	25.67	0.9508	261	25.65	0.9512
262	25.68	0.9518	263	25.67	0.9513
264	25.77	0.9509	265	25.71	0.9513
266	25.71	0.9518	267	25.77	0.9524
268	25.77	0.9519	269	25.82	0.9514
270	25.79	0.9508	271	25.79	0.9502
272	25.85	0.9508	273	25.82	0.9513
274	25.85	0.9518	275	25.85	0.9512
276	25.84	0.9507	277	25.88	0.9502
278	25.88	0.9507	279	25.88	0.9512
280	25.88	0.9507	281	25.88	0.9502
282	25.96	0.9497	283	25.93	0.9501
284	25.96	0.9495	285	25.96	0.9490
286	25.94	0.9485	287	25.99	0.9491
288	25.97	0.9486	289	26.03	0.9481
290	26.01	0.9476	291	25.99	0.9480
292	26.08	0.9486	293	26.04	0.9490
294	26.10	0.9484	295	26.08	0.9478
296	26.06	0.9472	297	26.12	0.9481
298	26.08	0.9476	299	26.14	0.9471

Continued on next page

TABLE II – continued from previous page

$A_{residual}$	Switchpoint (MeV)	Scaling Factor	$A_{residual}$	Switchpoint (MeV)	Scaling Factor
300	26.13	0.9478	301	26.08	0.9472

C. Gauss-Laguerre Quadrature

We added the option to use 8-point Gauss-Laguerre quadrature for high exciton number (> 15). Fig. 29 shows a comparison of the simple Gaussian and Gauss-Laguerre quadratures. Also notice that the NASA-Kalbach has much higher values of λ_j at the low end of the spectrum than the pure NASA. The purple dots are the 8-pt Gaussian quadrature and the black dots are the 8-pt Gauss-Laguerre quadrature. The Gaussian was exceptionally fortunate in that it struck the peak with its one low-end point. However, this leads to significant overestimation of λ_j down the tail. The Gauss-Laguerre underestimates the peak but then overestimates slightly along the tail. Even though it is clear this is not a very close fitting of λ_j , changing to a 10-pt Gauss-Laguerre only yielded a 0.2% difference. A future project could include investigating the behavior of λ_j across the variable landscape, and implementing an adaptive quadrature scheme. However, whatever numerical integration method we use must be fast as this integral is calculated hundreds of times for every event, and therefore billions of times for a typical simulation.

VII. RESULTS

Our preliminary results are promising. Fig. 30 displays the double differential cross section for the production of ${}^6\text{He}$ and ${}^7\text{Li}$ from the reaction 1200 MeV p + ${}^{197}\text{Au}$. The blue dashed lines are the expanded-MEM results (with the Dostrovsky cross section), and the red solid lines are results from the expanded-MEM with the upgraded NASA-Kalbach inverse cross section. The green points are experimental data by [20]. We see an improved accuracy in the particle spectra in the high-energy tails with the NASA inverse cross section.

For another example of our results, Fig. 31 plots the double differential cross section for the production of ${}^6\text{Li}$ and ${}^7\text{Be}$ from the reaction 200 MeV p + ${}^{59}\text{Co}$. Again notice the improved agreement with data in the high-energy tails. This reaction also highlights

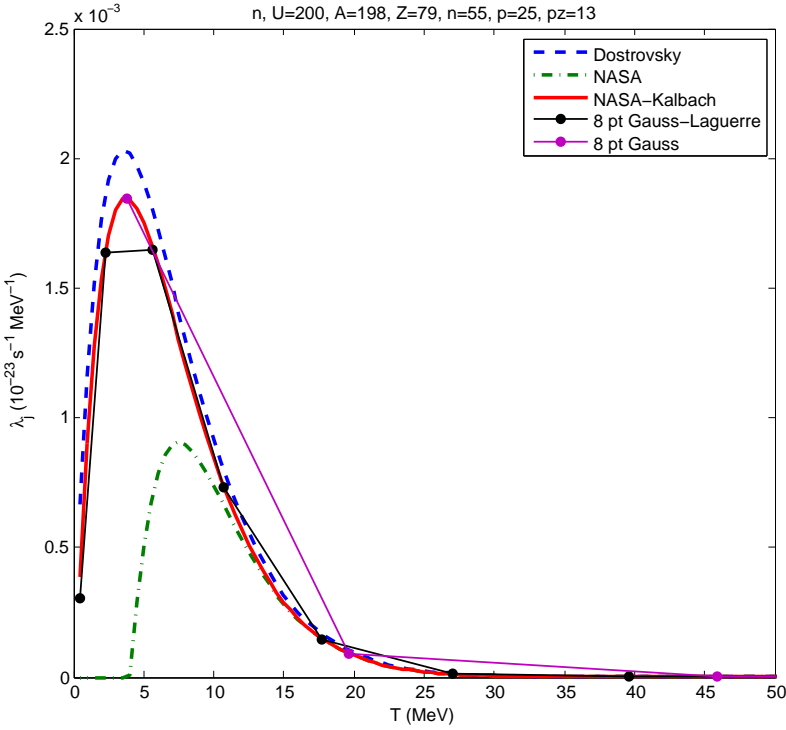


FIG. 29. λ_j as a function of the kinetic energy of the emitted neutron, from an excited ^{198}Au nucleus with $U = 200$ MeV and 55 excitons, 25 particle excitons, and 13 charged particle excitons.

the importance of eventually upgrading the inverse cross section used in the evaporation stage of CEM, as well. The evaporation stage produces the peak of the spectra, which for this reaction is too low, especially for ^7Be . With the implementation of the NASA inverse cross section in the preequilibrium stage we see improved agreement with data in the high-energy tails, but in order to achieve improved agreement in the peak we would need to also implement the NASA inverse cross section in the evaporation stage. We hope to do this in the future.

VIII. CONCLUSION

We upgraded the inverse cross section model in the preequilibrium stage of CEM03.03F to the NASA-Kalbach model. This included:

- Writing the NASA and coulomb barrier modules;
- Re-writing the Γ_j routines, including transforming them into modular Fortran;

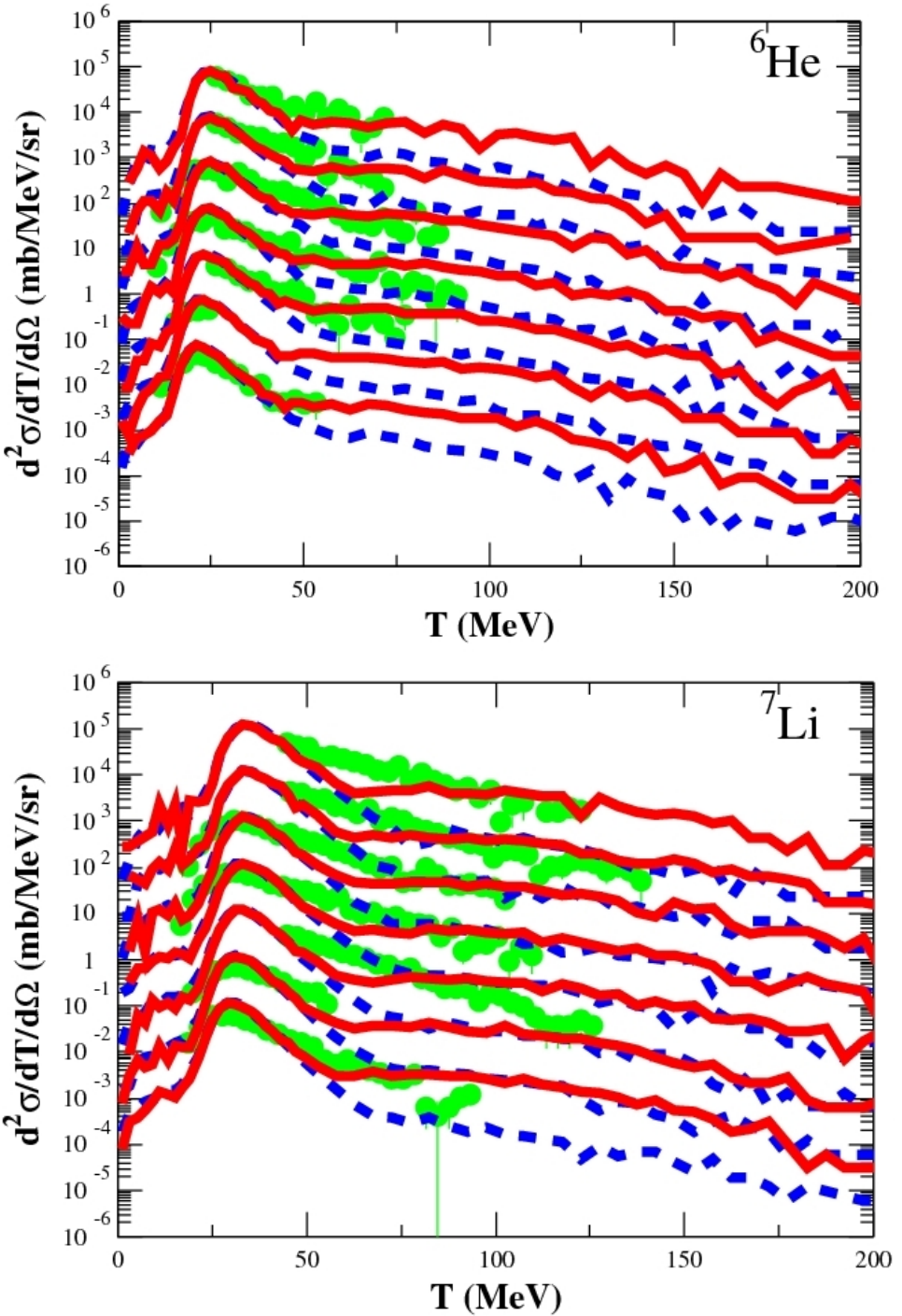


FIG. 30. Double differential cross section for the production of ${}^6\text{He}$ and ${}^7\text{Li}$ from the reaction 1200 MeV p + ${}^{197}\text{Au}$, for the angles of 15.6° , 20° , 35° , 50° , 65° , 80° , and 100° . The blue dashed lines are the expanded-MEM results (with the Dostrovsky inverse cross section), and the red solid lines are the expanded-MEM results with the NASA-Kalbach inverse cross section. The green points are experimental data by Budzanowski, *et al* [20].

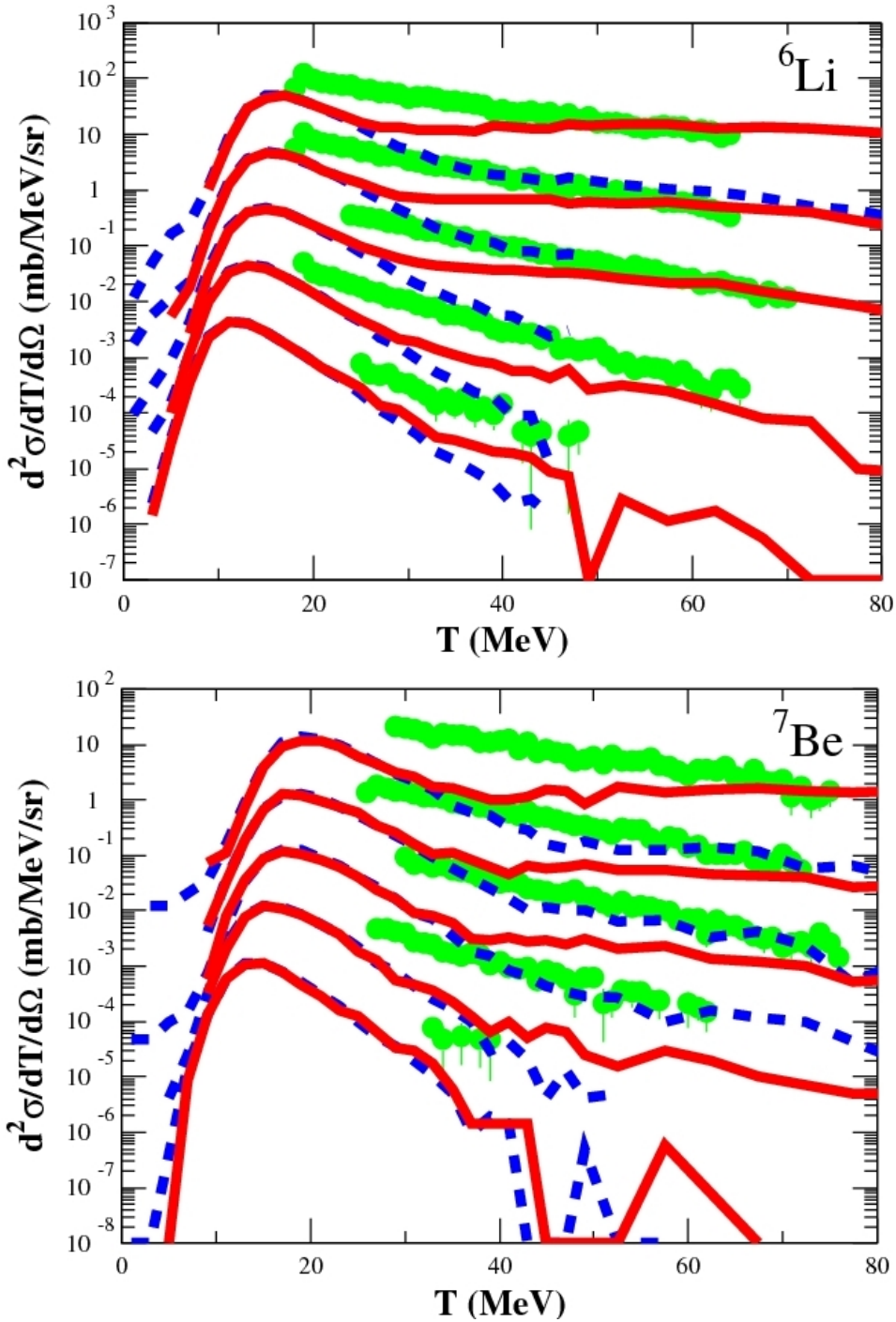


FIG. 31. Double differential cross section for the production of ${}^6\text{Li}$ and ${}^7\text{Be}$ from the reaction 200 MeV p + ${}^{59}\text{Co}$, for the angles of 20° , 45° , 60° , 90° , and 110° . The blue dashed lines are the expanded-MEM results (with the Dostrovsky inverse cross section), and the red solid lines are the expanded-MEM results with the NASA-Kalbach inverse cross section. The green points are experimental data by Machner, *et al* [19].

- Adding Kalbach systematics for low-energy neutrons;
- Adding Gauss-Laguerre quadrature for cases of high exciton number.

Our preliminary results are promising.

Future recommendations include:

- Re-parameterizing γ_j (sometimes called as γ_β);
- Investigating adaptive quadrature;
- Upgrading the inverse cross section used in the evaporation stage to the NASA-Kalbach cross section;
- Replacing GEM2 with a better evaporation/fission/fragmentation model.

There are several implications of this work on MCNP6. CEM03.03 is the default generator in MCNP6 for high-energy collisions induced by nucleon, pions, and gammas at energies up to several GeVs. Improvements to the CEM inverse cross sections should, therefore, result in improved prediction of particle spectra and total production cross sections, especially above ~ 100 MeV and for fragments heavier than ${}^4\text{He}$, among other results. In addition, MCNP6 uses the updated Barashenkov and Polanski (B&P) total reaction cross section systematics to simulate the mean-free path of neutrons, protons, and light fragments up to ${}^4\text{He}$. It uses a parameterization based on a geometric cross section for fragments heavier than ${}^4\text{He}$. Possible direct improvement of MCNP6 may be obtained by replacing the B&P model with NASA systematics and by replacing the geometric cross section approach with the better NASA model.

IX. ACKNOWLEDGMENTS

One of us (LMK) is grateful to

- a) Dr. Stepan Mashnik, for his continued mentoring and ample technical and scientific support and encouragement;
- b) Drs. Avneet Sood, Larry Cox, and Tim Goorley and Los Alamos National Laboratory for the opportunity to study with some of the world's greatest experts in nuclear physics, particularly high-energy physics.

- c) Dr. Akira Tokuhiro, for his continued support and expertise in serving as my thesis advisor.

This study was carried out under the auspices of the National Nuclear Security Administration of the U.S. Department of Energy at Los Alamos National Laboratory under Contract No. DE-AC52-06NA25396.

This work is supported in part (for L.M.K.) by the M. Hildred Blewett Fellowship of the American Physical Society, www.aps.org.

X. REFERENCES

- [1] S. G. Mashnik and A. J. Sierk, CEM03.03 User Manual, LANL Report, LA-UR-12-01364, Los Alamos (2012); <https://mcnp.lanl.gov/>.
- [2] T. Goorley, M. James, T. Booth, F. Brown, J. Bull, L. J. Cox, J. Durkee, J. Elson, M. Fensin, R. A. Forster, J. Hendricks, H. G. Hughes, R. Johns, B. Kiedrowski, R. Martz, S. Mashnik, G. McKinney, D. Pelowitz, R. Prael, J. Sweezy, L. Waters, T. Wilcox, and T. Zukaitis, Initial MCNP6 Release Overview, Nuclear Technology **180**, 298 (2012).
- [3] I. Dostrovsky, Z. Fraenkel, and G. Friedlander, Monte Carlo Calculations of Nuclear Evaporation Processes. III. Applications to Low-Energy Reactions, Phys. Rev. **116**, 683 (1959).
- [4] R. K. Tripathi, Francis A. Cucinotta, and John W. Wilson, Accurate universal parameterization of absorption cross sections, Nucl. Instr. Meth. B **117**, 347 (1996).
- [5] R. K. Tripathi, Francis A. Cucinotta, and John W. Wilson, Accurate universal parameterization of absorption cross sections II—neutron absorption cross sections, Nucl. Instr. Meth. B **129**, 11 (1997).
- [6] R. K. Tripathi, F. A. Cucinotta, J. W. Wilson, Universal parameterization of absorption cross sections III—light systems, Nucl. Instr. Meth. B **155**, 349 (1999).
- [7] Wen-qing Shen, Bing Wang, Jun Feng, Wen-long Zhan, Yong-tai Zhu, En-pu Feng, Total reaction cross section for heavy-ion collisions and its relation to the neutron excess degree of freedom, Nucl. Phys. A **491**, 130 (1989).
- [8] M. Takechi, M. Fukuda, M. Mihara, K. Tanaka, T. Chinda, T. Matsumasa, M. Nishimoto, R. Matsumiya, Y. Nakashima, H. Matsubara, K. Matsuta, T. Minamisono, T. Ohtsubo, T. Izumikawa, S. Momota, T. Suzuki, T. Yamaguchi, R. Koyama, W. Shinozaki, M. Takahashi,

- A. Takizawa, T. Matsuyama, S. Nakajima, K. Kobayashi, M. Hosoi, T. Suda, M. Sasaki, S. Sato, M. Kanazawa, and A. Kitagawa, Reaction cross sections at intermediate energies and Fermi-motion effect, Phys. Rev. C **79**, 061601 (2009).
- [9] Kei Iida, Akihisa Kohama, and Kazuhiro Oyamatsu, Formula for proton-nucleus reaction cross section at intermediate energies and its application, J. Phys. Soc. Japan **76**, 044201 (2007); arXiv:nucl-th/0601039.
- [10] A. Ingemarsson and M. Lantz, Geometrical aspects of reaction cross sections for ${}^3\text{He}$, ${}^4\text{He}$, and ${}^{12}\text{C}$ projectiles, Phys. Rev. C **67**, 064605 (2003).
- [11] H. H. K. Tang, G. R. Srinivasan, and N. Azziz, Cascade statistical model for nucleon-induced reactions on light nuclei in the energy range 50 MeV–1 GeV, Phys. Rev. C **42**, 1598 (1990).
- [12] C. Kalbach, Toward a global exciton model; lessons at 14 MeV, J. Phys. G: Nucl. Part. Phys. **24**, 847 (1998).
- [13] V. S. Barashenkov, A. Polanski, Electronic Guide for Nuclear Cross-Sections, Joint Institute for Nuclear Research Communication E2-94-417, JINR, Dubna, Russia (1994).
- [14] V. S. Barashenkov, W. Gudowski, and A. Polanski, Integral High-Energy Nucleon-Nucleus Cross Sections for Mathematical Experiments with Electronuclear Facilities, JINR Communication E2-99-207, JINR, Dubna, Russia (1990); private communications from Drs. Alexander Polanski and Dick Prael to SGM.
- [15] R. E. Prael, A. Ferrari, R. K. Tripathi, and A. Polanski, Comparison of Nucleon Cross Section Parametrization Methods for Medium and High Energies, LANL Report LA-UR-98-5813, Los Alamos (1998); Proc. Forth Int. Workshop on Simulating Accelerator Radiation Environments (SARE-4), Hyatt Regency, Knoxville, TN, September 13–16, 1998, edited by Tony A. Gabriel, Oak Ridge National Laboratory, pp. 171–181 (1999).
- [16] Stepan G. Mashnik and Leslie M. Kerby, MCNP6 fragmentation of light nuclei at intermediate energies, Nucl. Instr. Meth. A **764**, 59 (2014); arXiv:1404.7820.
- [17] Leslie M. Kerby, Stepan G. Mashnik, and Akira T. Tokuhiro, Production of Energetic Light Fragments with Expanded Cascade Exciton Model(CEM), Transactions of the American Nuclear Society **110**, 465 (2014).
- [18] L. M. Kerby, S. G. Mashnik, A. J. Sierk, Preequilibrium Emission of Light Fragments in Spallation Reactions, Nuclear Data Sheets **118**, 316 (2014); arXiv:1303.4311.

- [19] H. Machner, D. G. Aschman, K. Baruth-Ram, J. Carter, A. A. Cowley, F. Goldenbaum, B. M. Nangu, J. V. Pilcher, E. Sideras-Haddad, J. P. F. Sellschop, F. D. Smit, B. Spoelstra, and D. Steyn, Isotopic production cross sections in proton-nucleus collisions at 200 MeV, Phys. Rev. C **73**, 044606 (2006).
- [20] A. Budzanowski, M. Fidelus, D. Filges, F. Goldenbaum, H. Hodde, L. Jarczyk, B. Kamys, M. Kistryn, St. Kistryn, St. Kliczewski, A. Kowalczyk, E. Kozik, P. Kulessa, H. Machner, A. Magiera, B. Piskor-Ignatowicz, K. Pysz, Z. Rudy, R. Siudak, and M. Wojciechowski (PISA Collaboration) Competition of coalescence and “fireball” processes in nonequilibrium emission of light charged particles from $p+Au$ collisions, Phys. Rev. C **78**, 024603 (2008).
- [21] L. Sihver, A. Kohama, K. Iida, S. Hashimoto, H. Iwase, and K. Niita, Current status of the “Hybrid Kurotama model” for total reaction cross sections, Nucl. Instr. Meth. B **334**, 34 (2014).
- [22] L. Sihver, M. Lantz, M. Takechi, A. Kohama, A. Ferrari, F. Cerutti, and T. Sato, A comparison of total reaction cross section models used in particle and heavy ion transport codes, Adv. Space Res. **49**, 812 (2012).
- [23] V. Andersen, F. Ballarini, G. Battistoni, M. Campanella, M. Carboni, F. Cerutti, A. Empl, A. Fassò, A. Ferrari, E. Gadioli, M. V. Garzelli, K. Lee, A. Ottolenghi, M. Pelliccioni, L. S. Pinsky, J. Ranft, S. Roesler, P. R. Sala, and T. L. Wilson, The FLUKA code for space applications: recent developments, Adv. Space Res. **34**, 1302 (2004).
- [24] L. Sihver, C. H. Tsao, R. Silberberg, T. Kanai, and A.F. Barghouty, Total reaction and partial cross section calculations in proton-nucleus ($Z_t \leq 26$) and nucleus-nucleus reactions (Z_p and $Z_t \leq 26$), Phys. Rev. C **47**, 1225 (1993).
- [25] H. P. Wellisch and D. Axen, Total reaction cross section calculations in proton-nucleus scattering, Phys. Rev. C **54**, 1329 (1996).
- [26] L. Sihver, M. Lantz, T. T. Böhlen, A. Mairani, A. F. Cerutti, and A. Ferrari, A comparison of total reaction cross section models used in FLUKA, GEANT4, and PHITS, IEEE Aerospace Conf. pp 1-10 (2012); DOI: 10.1109/AERO.2012.6187014.
- [27] GEANT4 Physics Reference Manual, Chapter 23: Total Reaction Cross Section in Nucleus-Nucleus Reactions, gentoo.osuosl.org/distfiles/PhysicsReferenceManual-4.10.0.pdf. (2013).
- [28] A. Krylov, M. Paraipan, N. Sobolevsky, G. Timoshenko, and V. Tret'yakov, GEANT4, MCNPX, and SHIELD Code Comparison Concerning Relativistic Heavy Ion Interaction with

- Matter, Physics of Particles and Nuclei Letters **11**, 549 (2014).
- [29] K. K. Gudima, G. A. Ososkov, and V. D. Toneev, Model for Pre-Equilibrium Decay of Excited Nuclei, *Yad. Fiz.* **21** 260–272 (1975) [Sov. J. Nucl. Phys. **21** 138–143 (1975)].
 - [30] S. G. Mashnik and V. D. Toneev, MODEX – the Program for Calculation of the Energy Spectra of Particles Emitted in the Reactions of Pre-Equilibrium and Equilibrium Statistical Decays (text, in Russian; code, in FORTRAN66), JINR Communication P4-8417, Joint Institute for Nuclear Research, Dubna, USSR, 1974. 25 p; 2012 reprint, LANL Report LA-UR-12-20390, Los Alamos (2012), <https://mcnp.lanl.gov/>.
 - [31] S. Furihata, Statistical analysis of light fragment production from medium energy proton-induced reactions, *Nucl. Instr. Meth. B* **171**, 251 (2000); S. Furihata, K. Nita, S. Meigo, Y. Ikeda, and F. Maekawa, GEM code - a simulation program for the evaporation and the fission process of an excited nucleus, Japan Atomic Energy Res. Inst. (2001).
 - [32] Stepan G. Mashnik, Arnold J. Sierk, and Konstantin K. Gudima, Complex Particle and Light Fragment Emission in the Cascade-Exciton Model of Nuclear Reactions, LANL Report LA-UR-02-5185, Los Alamos (2002), Invited talk presented at the 12th Biennial Topical Meeting of the Radiation Protection and Shielding Division (RPSD) of the American Nuclear Society, April 14-17, 2002, Santa Fe, NM; E-print: nucl-th/0208048.
 - [33] S. G. Mashnik, R. E. Prael, and K. K. Gudima, Implementation of CEM03.01 into MCNP6 and its Verification and Validation Running through MCNP6. CEM03.02 Upgrade, LANL Research Note X-3-RN(U)-07-03, LANL Report LA-UR-06-8652, Los Alamos (2007); <https://mcnp.lanl.gov/>.
 - [34] R. E. Prael, A. Ferrari, R. K. Tripathi, and A. Polanski, Plots Supplimental to: Comparison of Nucleon Cross Section Parametrization Methods for Medium and High Energies, LANL Report LA-UR-98-5843, Los Alamos (December 16, 1998).
 - [35] T. W. Bonner and J. C. Slattery, Nonelastic Scattering Cross Sections for 8-20 MeV, *Phys. Rev.* **113**, 1088 (1959).
 - [36] J. R. Beyster, M. Walt, and E. W. Salmi, Interaction of 1.0-, 1.77-, 2.5-, 3.25-, and 7.0-MeV Neutrons with Nuclei, *Phys. Rev.* **104**, 1319 (1956).
 - [37] H. L. Taylor, O. Lönsjö, and T. W. Bonner, Nonelastic Scattering Cross Sections for Fast Neutrons, *Phys. Rev.* **100**, 174 (1955).

- [38] M. V. Pasechnik, Nonelastic Scattering of the Fast Neutrons, 1st UN Conf. Peaceful Uses Atomic Energy, Geneva 1955, **2**, 3 (1955).
- [39] J. R. Beyster, R. L. Henkel, R. A. Nobles, and J. M. Kister, Inelastic Collision Cross Sections at 1.0-, 4.0-, and 4.5-MeV Neutron Energies, Phys. Rev. **98**, 1216 (1955).
- [40] V. I. Strizhak, Inelastic Scattering Cross Sections of Nuclei for 2.5 MeV Neutrons, Soviet Physics - JETP **4**, 769 (1957).
- [41] L. E. Beghian, F. Hofman, and S. Wilensky, Measurement of Nonelastic Cross Section for Lead at 2.1 and 1.7 MeV, Neutron Cross-Section Techn. Conf., Washington 1966, **2**, 726 (1966).
- [42] G. C. Morrison, Inelastic Neutron Scattering, Physica (Utrecht) **22**, 1135 (1956).
- [43] Ju. G. Degtjarev, Nonelastic Cross Section for Neutrons with Nuclei by ^7Li , ^{12}C , ^{14}N , ^{26}Fe , Cu, Pb, ^{235}U , and ^{239}Pu , J. Nuclear Energy, Part A+B (Reactor Sci. Techn.) **20**, 818 (1966).
- [44] M. Walt and J. R. Beyster, Interaction of 4.1 MeV Neutrons with Nuclei, Phys. Rev. **98**, 677 (1955).
- [45] K. R. Poze and N. P. Glazkov, Inelastic Scattering of 0.3, 0.77, and 1.0 MeV Photoneutrons, Soviet Physics - JETP **3**, 745 (1956).
- [46] William P. Ball, Malcolm MacGregor, and Rex Booth, Neutron Nonelastic Cross Sections from 7 to 14 MeV, Phys. Rev. **110**, 1392 (1958).
- [47] H. A. Bethe, J. R. Beyster, R. F. Carter, Inelastic cross-sections for fission spectrum neutrons– IV, Journal of Nuclear Energy **4**, 147 (1957).
- [48] V. S. Barashenkov, *Cross Sections of Interaction of Particles and Nuclei with Nuclei*, (in Russian) JINR, Dubna, Russia (1993); tabulated data available at: <http://www.nea.fr/html/dbdata/bara.html>.
- [49] R. F. Carlson, Proton-Nucleus Total Reaction Cross Sections and Total Cross Sections Up to 1 GeV Atomic Data and Nuclear Data Tables **63**, 93 (1996).
- [50] A. Ingemarsson, Nyberg, P. U. Renberg, O. Sundberg, R.F. Carlson, A. Auce, R. Johansson, G. Tibell, B. C. Clark, L. Kurth Kerr, S. Hama, Reaction cross sections for 65 MeV protons on targets from ^9Be to ^{208}Pb , Nucl.Phys.**A653**, 341 (1999).
- [51] N. Okumura, Y. Aoki, T. Joh, Y. Honkyu, K. Hirota, K. S. Itoh, Measuring system of proton total reaction cross-sections at tandem energy region, Nucl. Instr. Meth. A **487**, 565 (2002).

- [52] R. E. Warner, R. A. Patty, P. M. Voyles, A. Nadasen, F. D. Becchetti, J. A. Brown, H. Esbensen, A. Galonsky, J. J. Kolata, J. Kruse, M. Y. Lee, R. M. Ronningen, P. Schwandt, J. von Schwarzenberg, B. M. Sherrill, K. Subotic, J. Wang, and P. Zecher, Total reaction and 2n-removal cross sections of 20-60A MeV $^{4,6,8}\text{He}$, $^{6-9,11}\text{Li}$, and ^{10}Be on Si, Phys. Rev. C **54**, 1700 (1996).
- [53] V.Yu. Uglyumov, I. V . Kuznetsov, E. Bialkowski, A. Kugler, K. A. Kuterbekov, I. N. Kuhtina, V. F. Kushniruk, V. G. Lyapin, V. A. Maslov, Yu. E. Penionzhkevich, Yu. G. Sobolev, W. Trzaska, G. P. Tjurin, S. V. Khlebnikov, and S. Yamaletdinov, Energy Dependence of the Total Cross Section for the Reaction of ^4He Ions with Silicon Nuclei, Physics of Atomic Nuclei **68**, 16 (2005) [Yad. Fiz. **68**, 17 (2005)].
- [54] V. Yu Uglyumov, I. V Kuznetsov, K. B Basybekov, E. Bialkowski, A. Budzanowski, A. Duysebaev, B. A Duysebaev, T. K. Zholybaev, K. M. Ismailov, K. K. Kadyrzhanov, R. Kalpakchieva, A. Kugler, I. N. Kukhtina, V. F. Kushniruk, K.A. Kuterbekov, A. Mukhambetzhan, Yu. E. Penionzhkevich, B.M. Sadykov, I. Skwirczynska, and Yu. G Sobolev, Total reaction cross section for ^4He collisions with silicon in the energy range 3-10 MeV/u, Nucl. Phys. A **734**, E53 (2004).
- [55] A. Ingemarsson, J. Nyberg, P. U. Renberg, O. Sundberg, R. F. Carlson, A. J. Cox, A. Auce, R. Johansson, G. Tibell, Dao T. Khoa, R. E. Warner, New results for reaction cross sections of intermediate energy α -particles on targets from ^9Be to ^{208}Pb , Nucl. Phys. A **676**, 3 (2000).
- [56] M. K. Baktybaev, A.Duissebaev, B . A. Duisebaev, K. M. Ismailov, M. G. Itkis, K. K. Kadyrzhanov, R. Kalpakchieva, I. V. Kuznetsov, K. A. Kuterbekov, I. N. Kukhtina, S. M. Lukyanov, A. Mukhamedzhan, Yu. E. Penionzhkevich, B. M. Sadykov, Yu. G. Sobolev, and V. Yu. Uglyumov, Total Reaction Cross Section from the Interaction of ^4He Ions with ^{28}Si at 10-30 MeV, Physics of Atomic Nuclei **66**, 1615 (2003) [Yad. Fiz. **66**, 1662 (2003)].
- [57] R. E. Warner, M. H. McKinnon, N. C. Shaner, F. D. Becchetti, A. Nadasen, D. A. Roberts, J. A. Brown, A. Galonsky, J. J. Kolata, R. M. Ronningen, M. Steiner, and K. Subotic, Total reaction and neutron-removal cross sections of (30-60)A MeV He and Li isotopes on Pb, Phys. Rev. C **62**, 024608 (2000).
- [58] A. Auce, R. F. Carlson, A. J. Cox, A. Ingemarsson, R. Johansson, P. U. Renberg, O. Sundberg, G. Tibell, and R. Zorro, Reaction cross sections for 75-190 MeV alpha particles on targets from ^{12}C to ^{208}Pb , Phys. Rev. C **50**, 871 (1994).

- [59] B. Bonin, N. Alamanos, B. Berthier, G. Bruge, H. Faraggi, J. C. Lugol, W. Mittig, L. Papineau, A. I. Yavin, J. Arvieux, L. Farvacque, M. Buenerd, and W. Bauhoff, Alpha-nucleus elastic scattering at intermediate energies, Nucl.Phys.A **445**, 381 (1985).
- [60] N. Keeley, S. J. Bennett, N. M. Clarke, B. R. Fulton, G. Tungate, P. V. Drumm, M. A. Nagarajan, J. S. Lilley, Optical model analyses of $^{6,7}\text{Li} + ^{208}\text{Pb}$ elastic scattering near the Coulomb barrier, Nucl. Phys. A **571**, 326 (1994).
- [61] R. E. Warner, M. H. McKinnon, J. S. Needleman, N. C. Shaner, F. D. Becchetti, D. A. Roberts, A. Galonsky, R. M. Ronningen, M. Steiner, J. A. Brown, J. J. Kolata, A. Nadasen, and K. Subotic, Total reaction and neutron-removal cross sections of (30-60)A MeV Be isotopes on Si and Pb, Phys. Rev. C **64**, 044611 (2001).
- [62] . E. Warner, F. Carstoiu, J. A. Brown, F. D. Becchetti, D. A. Roberts, B. Davids, A. Galonsky, R. M. Ronningen, M. Steiner, M. Horoi, J. J. Kolata, A. Nadasen, C. Samanta, J. Schwartzenberg, and K. Subotic, Reaction and proton-removal cross sections of ^6Li , ^7Be , ^{10}B , $^{9,10,11}\text{C}$, ^{12}N , $^{13,15}\text{O}$, and ^{17}Ne on Si at 15 to 53 MeV/nucleon, Phys. Rev. C **74**, 014605 (2006).
- [63] C. Borcea, F. Carstoiu, F. Negoita, M. Lewitowicz, M. G. Saint-Laurent, R. Anne, D. Bazin, V. Borrel, J. M. Corre, Z. Dlouhy, A. Fomitchev, D. Guillemaud-Mueller, H. Keller, A. Kordyasz, S. Lukyanov, A. C. Mueller, Yu. Penionzhkevich, P. Roussel-Chomaz, N. Skobelev, O. Sorlin, O. Tarasov, ^8B studied as a secondary beam at GANIL, Nucl. Phys. A **616**, 231 (1997).
- [64] A. C. C. Villari, W. Mittig, E. Plagnol, Y. Schutz, M. Lewitowicz, L. Bianchi, B. Fernandez, J. Gastebois, A. Gillibert, C. Stephan, L. Tassan-Got, G. Audi, Wenlong Zhan, A. Cunsolo, A. Foti, A. Belezyorov, S. Lukyanov, and Y. Penionzhkevich, Measurements of reaction cross sections for neutron-rich exotic nuclei by a new direct method, Phys. Lett. B **268**, 345 (1991).
- [65] A. Khouaja, A. C. C. Villari, M. Benjelloun, D. Hirata, G. Auger, H. Savajols, W. Mittig, P. Roussel-Chomaz, N. A. Orr, M. G. Saint-Laurent, S. Pita, A. Gillibert, M. Chartier, C. E. Demonchy, L. Giot, D. Baiborodin, Y. Penionzhkevich, W. N. Catford, A. Lépine-Szily, and Z. Dlouhy, Reaction cross-section and reduced strong absorption radius measurements of neutron-rich nuclei in the vicinity of closed shells $N = 20$ and $N = 28$, Nucl. Phys. A **780**, 1 (2006).
- [66] Michael G. Mazarakis and William E. Stephens, Experimental Measurements of the $^{12}\text{C} + ^{12}\text{C}$ Nuclear Reactions at Low Energies, Phys Rev. C **7**, 1280 (1973).

- [67] C. Zeitlin, S. Guetersloh, L. Heilbronn, J. Miller, A. Fukumura, Y. Iwata, and T. Murakami, Fragmentation cross sections of 290 and 400 MeV/nucleon ^{12}C beams on elemental targets, Phys. Rev. C **76**, 014911 (2007).
- [68] A. N. Golovchenko, J. Skvarč, N. Yasuda, M. Giacomelli, S. P. Tretyakova, R. Ilić, R. Bimbot, M. Toulemonde, and T. Murakami, Total charge-changing and partial cross-section measurements in the reactions of \sim 110-250 MeV/nucleon ^{12}C in carbon, paraffin, and water, Phys. Rev. C **66**, 014609 (2002).
- [69] E. Betak, Complex Particle Emission in the Exciton Model of Nuclear Reactions, Acta Phys. Slov. **26**, 21 (1976).
- [70] J. R. Wu and C. C. Chang, Complex-Particle Emission in the Pre-Equilibrium Exciton Model, Phys. Rev. C **17**, 1540 (1978).